Heterogeneous ice nucleation and water uptake by field-collected atmospheric particles below 273 K

Bingbing Wang,[1] Alexander Laskin,[2] Tobias Roedel,[3] Mary K. Gilles,[3] Ryan C. Moffet,[3] Alexei V. Tivanski,[4] and Daniel A. Knopf[1]

Received 6 January 2012; revised 1 August 2012; accepted 16 August 2012; published 25 September 2012.

[1] Ice formation induced by atmospheric particles through heterogeneous nucleation is not well understood. Onset conditions for heterogeneous ice nucleation and water uptake by particles collected in Los Angeles and Mexico City were determined as a function of temperature (200–273 K) and relative humidity with respect to ice (RH_{ice}). Four dominant particle types were identified including soot associated with organics, soot with organic and inorganics, inorganic particles of marine origin coated with organic material, and Pb/Zn-containing particles apportioned to emissions relevant to waste incineration. Single particle characterization was provided by micro-spectroscopic analyses using computer controlled scanning electron microscopy with energy dispersive analysis of X-rays (CCSEM/EDX) and scanning transmission X-ray microscopy with near edge X-ray absorption fine structure spectroscopy (STXM/NEXAFS). Above 230 K, significant differences in onsets of water uptake and immersion freezing of different particle types were observed. Below 230 K, particles exhibited high deposition ice nucleation efficiencies and formed ice at RH_{ice} well below homogeneous ice nucleation limits. The data suggest that water uptake and immersion freezing are more sensitive to changes in particle chemical composition compared to deposition ice nucleation. The data demonstrate that anthropogenic and marine influenced particles, exhibiting various chemical and physical properties, possess distinctly different ice nucleation efficiencies and can serve as efficient IN at atmospheric conditions typical for cirrus and mixed-phase clouds.

Citation: Wang, B., A. Laskin, T. Roedel, M. K. Gilles, R. C. Moffet, A. V. Tivanski, and D. A. Knopf (2012), Heterogeneous ice nucleation and water uptake by field-collected atmospheric particles below 273 K, *J. Geophys. Res.*, *117*, D00V19, doi:10.1029/2012JD017446.

1. Introduction

[2] Atmospheric particles can affect the global radiative budget directly, by scattering and absorption of solar and terrestrial radiation, and indirectly by aerosol-cloud interactions [*Twomey*, 1974; *Albrecht*, 1989; *Baker*, 1997; *Rosenfeld*, 2000; *Ramanathan et al.*, 2001; *Forster et al.*, 2007; *Baker and Peter*, 2008]. The latter can lead to formation of new clouds. It can also modify the microphysical and the radiative properties, amount, and lifetime of clouds. These indirect effects pose one of the largest uncertainties in predicting climate change [*Forster et al.*, 2007]. The ability of airborne particles to provide surfaces for ice formation, i.e. acting as ice nuclei (IN), is not well understood [*Baker*, 1997; *Cantrell and Heymsfield*, 2005; *Forster et al.*, 2007; *Baker and Peter*, 2008]. Ice crystals can affect the global radiation budget, the hydrological cycle, and the water vapor distribution in the atmosphere [*Lohmann and Roeckner*, 1995; *Chen et al.*, 2000; *Held and Soden*, 2000; *Verlinde et al.*, 2007; *Avramov and Harrington*, 2010]. In this study, heterogeneous ice nucleation efficiency of atmospheric particles collected during the CalNex (California Research at the Nexus of Air Quality and Climate Change) (http://esrl.noaa.gov/csd/calnex/) and MILAGRO (Megacity Initiative: Local and Global Research Observations) [*Molina et al.*, 2007] field studies were investigated.

[3] In the atmosphere, ice formation is initiated by homogeneous or heterogeneous nucleation [*Pruppacher and Klett*, 1997]. Homogeneous ice nucleation proceeds from supercooled aqueous droplets below ~235 K [*Koop et al.*, 2000a]. Heterogeneous ice nucleation can take place on pre-existing

[1]Institute for Terrestrial and Planetary Atmospheres, School of Marine and Atmospheric Sciences, State University of New York at Stony Brook, Stony Brook, New York, USA.
[2]William R. Wiley Environmental Molecular Sciences Laboratory, Pacific Northwest National Laboratory, Richland, Washington, USA.
[3]Chemical Sciences Division, Lawrence Berkeley National Laboratory, Berkeley, California, USA.
[4]Department of Chemistry, University of Iowa, Iowa City, Iowa, USA.

Corresponding author: D. A. Knopf, Institute for Terrestrial and Planetary Atmospheres, School of Marine and Atmospheric Sciences, State University of New York at Stony Brook, Stony Brook, NY 11794, USA. (daniel.knopf@stonybrook.edu)

©2012. American Geophysical Union. All Rights Reserved.
0148-0227/12/2012JD017446

IN via different nucleation pathways: (a) deposition mode in which ice crystals form on IN directly from the supersaturated vapor phase, (b) immersion freezing in which ice crystals form from IN immersed in supercooled aqueous droplets, (c) condensation freezing in which ice crystals form during the condensation of water vapor onto IN at supersaturated conditions, and (d) contact freezing in which ice formation is triggered by collision of supercooled droplets with insoluble particles [*Vali*, 1985; *Pruppacher and Klett*, 1997].

[4] This study focuses on heterogeneous ice nucleation induced by various types of field-collected particles. Classical nucleation theory (CNT) states that the presence of an ice nucleus reduces the Gibbs free energy for the formation of a critical ice embryo. For this reason, heterogeneous ice nucleation proceeds at warmer temperatures and lower supersaturations than homogeneous ice nucleation [*Pruppacher and Klett*, 1997]. Heterogeneous ice nucleation plays an important role in formation of cirrus and mixed-phase clouds (i.e., the coexistence of ice crystals and supercooled aqueous droplets) by modifying the number and shapes of ice crystals [*Hallett et al.*, 2002; *Bailey and Hallett*, 2004; *Avramov and Harrington*, 2010]. This will lead to subsequent important consequences for cloud evolution and radiative properties [*Jensen and Toon*, 1997; *Kärcher and Ström*, 2003; *McFarquhar et al.*, 2007].

[5] Field measurements have shown that particles consisting of organic and inorganic compounds, such as soot, sulfate, sea salt, or metals, can reach altitudes where temperatures favor ice formation [*Murphy et al.*, 1998; *DeMott et al.*, 2003; *Cziczo et al.*, 2004; *Jost et al.*, 2004; *Murphy et al.*, 2007a; *Cziczo et al.*, 2009; *Froyd et al.*, 2010]. Previous cirrus and mixed-phase cloud studies also found that ice crystal residues can contain organic material and, in some cases, metal-bearing particles [*Chen et al.*, 1998; *DeMott et al.*, 2003; *Cziczo et al.*, 2004, 2009; *Froyd et al.*, 2010; *Prenni et al.*, 2009a; *Ebert et al.*, 2011].

[6] In the atmosphere, secondary organic aerosols (SOAs) are ubiquitous and can account for a large mass fraction of the organic particles [*Kanakidou et al.*, 2005; *Zhang et al.*, 2007]. SOA are formed by photochemical processing of anthropogenic and biogenic volatile organic compounds (VOCs). The chemical and physical properties of SOA can affect their interactions with water vapor [*Kanakidou et al.*, 2005; *Fuzzi et al.*, 2006; *Hallquist et al.*, 2009; *Koop et al.*, 2011]. For example, oxidation level of SOA affects particle hygroscopicity [*Jimenez et al.*, 2009; *Massoli et al.*, 2010] and viscosity of SOA can govern the diffusion of water molecules into the particle [*Mikhailov et al.*, 2009; *Virtanen et al.*, 2010; *Koop et al.*, 2011]. Recently, *Virtanen et al.* [2010] inferred that these SOA can be present as amorphous (non-crystalline) solid particles. When exposed to low temperatures, aqueous organic particles can form glasses which are disordered amorphous solids [*Murray*, 2008; *Zobrist et al.*, 2008, 2011; *Koop et al.*, 2011]. During transport, aerosol particles can undergo various atmospheric aging processes including, but not limited to: (1) condensation of SOA due to photochemical processing of VOCs [*Seinfeld and Pandis*, 1998; *Kanakidou et al.*, 2005], (2) heterogeneous oxidation by atmospheric trace gases such as O_3, NO_3, and OH which can lead to the formation of hydrophilic functional groups on the particle surfaces [*Akhter et al.*, 1985; *Smith et al.*, 1988; *Chughtai et al.*, 1991; *Kanakidou et al.*, 2005; *Zuberi et al.*, 2005; *Knopf et al.*, 2006; *Rudich et al.*, 2007; *Daly and Horn*, 2009; *Springmann et al.*, 2009; *George and Abbatt*, 2010; *Knopf et al.*, 2011a; *Kaiser et al.*, 2011], and (3), condensation of hydrophilic material such as inorganic acids, i.e., H_2SO_4 and HNO_3 [*Jang et al.*, 2002; *Riemer et al.*, 2004; *George and Abbatt*, 2010]. Modifications of surface chemistry can affect the particles' hygroscopicities and ice nucleation efficiencies. Most previous studies have investigated the effects of aging processes on ice nucleation using laboratory generated particles [*Garten and Head*, 1964; *Möhler et al.*, 2005; *Dymarska et al.*, 2006; *Möhler et al.*, 2008; *Koehler et al.*, 2009; *Prenni et al.*, 2009b; *Sullivan et al.*, 2010; *Friedman et al.*, 2011; *Wang and Knopf*, 2011; *Niedermeier et al.*, 2011].

[7] *Murphy et al.* [2007b] showed that in the eastern and western United States up to 25% of particles with 0.25 and 3 μm in diameter which have been sampled by airborne and surface-based instruments contain trace amounts of Pb. Pb-containing particles emitted from various sources, including biomass burning and industrial pollution, contain other metals, most often Zn [*Murphy et al.*, 2007b]. *Borys and Duce* [1979] found only a weak correlation between Pb and IN concentrations which were measured using a thermal diffusion chamber at 256 K. They concluded that no interrelationship between lead or iodine and IN exists [*Borys and Duce*, 1979]. However, more recent studies indicated that the number fraction of Pb-containing particles was enhanced in ice crystal residues collected from mixed-phase clouds [*Cziczo et al.*, 2009; *Ebert et al.*, 2011]. *Moffet et al.* [2008] showed that Pb/Zn-containing particles represented a high fraction of particles emitted from waste incineration. To study the potential impacts of metal-containing particles on cloud formation, the ice nucleation efficiency and water uptake behavior of metal-containing particles are also investigated in this study.

[8] In this study, we combine optical microscope measurements of ice nucleation with micro-spectroscopy particle analyses and discuss ice nucleation observations in a context of overall trends in particle composition and sources. The experimental approach is organized as follows: (1) particle collection in the field, (2) single particle analyses, and (3) water uptake and ice nucleation onset experiments using an optical microscope coupled to an ice nucleation cell. CCSEM/EDX, STXM/NEXAFS, and water uptake/ice nucleation experiments were conducted over the same sample of particles collected on three co-located substrates as illustrated by Figure S1 in the auxiliary material.[1] The analyses of particles were conducted on particle samples which were collected at the same time from same air flow. Observed trends in ice nucleation and water uptake onsets at low temperature were related to overall variability in particle composition and morphology. Deposition ice nucleation was analyzed with regard to classical nucleation theory, singular hypothesis, and IN activated fraction providing estimates of heterogeneous ice nucleation rate coefficients, J_{het}, cumulative IN spectra, K,

[1]Auxiliary materials are available in the HTML. doi:10.1029/2012JD017446.

Table 1. The Sampling Location, Sampling Time (Local Time), Number of Particles Analyzed by CCSEM/EDX and STXM/NEXAFS, Mean Particle Size in Diameter, Particle Number Density on the Substrate, Total Particle Number and Surface Area of Particles Available for Ice Nucleation Experiment of Respective Samples

Location and Sampling Date	Sample and Sampling Time	Number of Analyzed Particles		Mean Diameter (μm)	Number Density ($\times 10^6$ mm^{-2})	Number ($\times 10^6$)	Surface Area ($\times 10^{-2}$ cm^2)
		CCSEM/EDX	STXM/NEXAFS				
Los Angeles, May 19, 2010	A2, 06–12	2580	792	0.32	2.3	1.6	0.26
	A3, 12–18	5440	786	0.37	1.6	1.1	0.24
	A4, 18–24	7602	N/A	0.39	1.8	1.0	0.24
Los Angeles, May 23, 2010	B2, 06–12	2214	590	0.47	0.8	0.5	0.18
	B4, 18–24	2140	368	0.26	0.6	0.9	0.09
Mexico City, March 24, 2006	M1, ~05	4400[a]	800[b]	0.52	0.2	0.2	0.05

[a]See text and *Moffet et al.* [2008] for details.
[b]Number of particles analyzed by ATOFMS; see text and *Moffet et al.* [2008] for details.

IN activated fraction, and potential ambient IN number concentrations as given in the auxiliary material.

2. Experimental Setup

2.1. Particle Collection

[9] Six particle samples were selected for investigation of water uptake and ice nucleation onsets. The sampling time and location, particle size, particle number density, and total particle number and surface area available for ice nucleation of the six investigated field-collected samples are summarized in Table 1. To investigate the potential differences in water uptake and ice nucleation efficiency by particles from anthropogenic and marine sources, three sets of samples were selected for this study. These include samples with mainly soot particles associated with either organics or organics and inorganics (A2, A3, and A4 samples), mainly inorganic particles of marine origin coated with organic coatings (B2 and B4 samples), and Pb/Zn-containing inorganic particles, mixed with soot and a minor presence of organic material, from anthropogenic urban emissions apportioned to waste incineration (M1 sample) [*Moffet et al.*, 2008].

[10] Samples A (A2, A3, A4) and B (B2, B4) were collected at the ground sampling site during the CalNex campaign on May 19 and May 23, respectively. The observed meteorological conditions and air parcel backward trajectories calculated using the Hybrid Single-Particle Lagrangian Integrated Trajectory (HYSPLIT) Model (R. R. Draxler and G. D. Rolph, HYSPLIT Model, 2012, access via NOAA ARL READY, http://ready.arl.noaa.gov/HYSPLIT.php) during the sampling periods are given in the auxiliary material (Figures S2 and S3, Table S1, and Text S1). A cascade Multi Orifice Uniform Deposition Impactor (MOUDI) was used to collect size-selected aerosol samples over 6 hour time periods. The particle samples used in this study were collected at the 8th stage of the MOUDI with 50% cut off diameter of 0.32 μm on a set of pre-arranged substrates as illustrated by Figure S1 in the auxiliary material: (a) Si_3N_4 coated silicon wafer chips for ice nucleation experiments, (b) silicon wafers with Si_3N_4 window for particle analysis using STXM/NEXAFS, and (c) transmission electron microscopy (TEM) grids (copper 400 mesh grids, carbon type B film, Ted Pella, Inc.) for CCSEM/EDX analysis. M1 sample was collected using a compact Time Resolved Aerosol Collector (TRAC) on Si_3N_4 coated silicon wafer chip within Mexico City at the T0 sampling site on March 24, 2006 during the MILAGRO campaign [*Laskin et al.*, 2006; *Moffet et al.*, 2008, 2010a; *DeMott et al.*, 2010].

2.2. Particle Analyses

2.2.1. CCSEM/EDX Analysis

[11] The computer controlled scanning electron microscopy (CCSEM) with energy dispersive X-rays (EDX) microanalysis provides information on size and elemental composition of individual particles [*Laskin et al.*, 2003, 2006]. Particles are first imaged and the acquired images are used for determinations of particle size and morphology. Then, each of the detected particles is ablated again by the electron beam and EDX spectra of individual particles are recorded and processed yielding the elemental composition. A SEM (Quanta 3D model, FEI, Inc.) with a 10 mm^2 Si(Li) X-ray detector (EDAX, Inc.) was used in this study. The elements considered in the X-ray analysis were C, N, O, Na, Mg, Al, Si, P, S, Cl, K, Ca, Mn, Fe, Zn for samples collected during the CalNex campaign. Additional descriptions of the applied method are published elsewhere [*Laskin et al.*, 2003, 2006; *Moffet et al.*, 2008, 2010a].

2.2.2. STXM/NEXAFS Analysis

[12] STXM utilizes the soft X-ray beam generated from the synchrotron light sources to probe the particles. STXM measures the transmitted X-rays by raster scanning the sample at a given photo energy to obtain an image [*Kilcoyne et al.*, 2003]. Spatially resolved X-ray spectra are measured as a function of photon energy over the sample area. Chemical composition of individual particles within the sample area can be identified by analyzing the recorded spectra [*Moffet et al.*, 2008, 2010a, 2010b]. Particle samples were analyzed using STXM/NEXAFS at beamlines 5.3.2 and 11.0.2 of the Light Source in Lawrence Berkeley National Laboratory. STXM/NEXAFS has a spatial resolution of 25 to 35 nanometers depending upon the used zone plate. STXM/NEXAFS analysis at the carbon K-edge provides spatial mapping of the chemical composition which allows identification of three constituents including organic carbon (OC), elemental carbon (EC, i.e. soot), and inorganic components (In) within individual particles. An overview of the application of this technique to atmospheric aerosols can be found in a recent review by *Moffet et al.* [2010c] and technical details on STXM are published elsewhere [*Kilcoyne et al.*, 2003; *Ghorai and Tivanski*, 2010; *Ghorai et al.*, 2011].

[13] Particle mixing state can be determined from spatial maps of chemical composition [*Moffet et al.*, 2008, 2010a, 2010b]. Samples A2, A3, B2, and B4 contained particles

smaller than ~200 nm in diameter. Identifying these small, weakly absorbing particles was ambiguous, in particular for B2 and B4 samples that contained very little carbon. Within each sample, the percentage of chemically unidentified particles (smaller than 200 nm) to the total number of particles was: A2 (27%), A3 (24%), B2 (22%), and B4 (63%). For consistency, particles with diameters smaller than ~200 nm were not included in the summary of STXM/NEXAFS analysis. However, more than 90% of observed ice nucleation events occurred on particles larger than 200 nm. Thus, the unidentified particles in each sample do not contribute a significant fraction of observed ice nucleation events.

2.3. Ice Nucleation Apparatus

[14] Ice nucleation and water uptake of aerosol particles were determined using a custom-built apparatus consisting of an optical microscope (OM) and an ice nucleation cell (INC). The OM allowed the determination of particle size and phase whereas the INC allowed for samples to be exposed to an environment in which temperature and relative humidity with respect to water (RH) were carefully controlled. Onset conditions (temperature and RH_{ice}) for water uptake and the first ice nucleation event initiated by the deposited particles were determined according to the changes in particle size and phase. The INC allows the exposure of aerosol particles to temperatures (T_p) as low as 200 K and RH_{ice} up to water saturation [*Knopf et al.*, 2010, 2011b; *Wang and Knopf*, 2011]. The experimental method has been described in previous studies in detail [*Knopf et al.*, 2010, 2011b; *Wang and Knopf*, 2011] and is only presented briefly here.

2.3.1. Experimental Procedure

[15] Samples were placed inside the INC, where the entire sample area was optically monitored and the changes in particle phase and size were digitally recorded using OM in reflected light mode. Particles were exposed to a humidified N_2 (ultra high purity) gas flow at about 1 standard liter per minute (SLPM) with a constant dew point temperature (T_d) generated by passing N_2 gas through a temperature controlled water reservoir [*Wang and Knopf*, 2011]. At the exit of the INC, T_d was determined using a chilled mirror hygrometer (GE Sensing) in a range of 203–293 K with an uncertainty of better than ±0.15 K [*Knopf and Lopez*, 2009; *Knopf et al.*, 2010, 2011b; *Wang and Knopf*, 2011]. Once T_d was stable, T_p was adjusted. The particles were then cooled at a rate of 0.1 K min^{-1}, corresponding to an increase in RH_{ice} of ~2.3 to 1.5% per minute for temperatures from 200 to 260 K, and exposed to ice saturation until ice formation or water uptake was observed [*Dymarska et al.*, 2006; *Eastwood et al.*, 2008; *Wang and Knopf*, 2011].

[16] Optical images of the sample, T_d, and T_p were recorded every 0.02 K (~12 s). The OM allowed for visual identification of water uptake or ice formation when changes in particle phase or size larger than 0.2 and 1 μm using a magnification of 1130× and 230×, respectively. RH_{ice} and RH above the particles were calculated from monitored T_p and T_d using the parameterizations for water vapor pressures given by *Murphy and Koop* [2005]. If two or more ice crystals formed simultaneously, then all ice crystals were counted [*Wang and Knopf*, 2011]. Subsequent ice formation events were discarded since a uniform water vapor field may not persist when ice crystals are present in the INC [*Wang and Knopf*, 2011]. Reported onset values represent the first observed appearance of water or ice associated with particles. Observed ice formation on blank substrates indicate the maximum RH_{ice} values for which the substrates do not affect ice nucleation [*Knopf et al.*, 2010] as shown below. In addition, ice formation initiated by particles or substrate can be visually distinguished in the recorded images. Reported onsets of water uptake and ice nucleation were only those initiated by particles. T_p was calibrated against T_d measured from the hygrometer since in equilibrium conditions $T_p = T_d$ as described in detail by *Wang and Knopf* [2011]. Experimental uncertainties were calculated from the maximum difference between T_p and T_d due to the given uncertainties of $\Delta T_d < \pm 0.15$ K and $\Delta T_p < \pm 0.3$ K resulting in a conservative uncertainty of $\Delta RH_{ice} < \pm 11\%$ at 200 K and $\Delta RH_{ice} < \pm 3\%$ at 260 K [*Knopf et al.*, 2010; *Wang and Knopf*, 2011]. Error bars presented in this manuscript represent one standard deviation of observed RH_{ice} and T_p onsets for ice nucleation and water uptake obtained from multiple experiments. For all samples, at least 3 experiments were conducted at each investigated temperature. In total, about 330 ice nucleation experiments were performed.

[17] At higher temperatures, i.e., above 230 K, water uptake and immersion freezing may occur and lead to a change of particle morphology which may change the ice nucleation efficiencies. To investigate the potential effects of morphology changes due to water uptake on deposition ice nucleation, we conducted the experiment according to the following procedure. First, deposition ice nucleation experiments were performed at temperatures below 225 K. Then, immersion freezing experiments which involved water uptake were conducted at higher temperatures. Subsequently, deposition ice nucleation experiments at lower temperatures were repeated to observe changes in the ice nucleation onset due to potentially altered particles. Prior to deposition ice nucleation experiments, the particles were conditioned at 275 K and $RH_{ice} < 1\%$ for more than 5 min to remove potential particle preactivation [*Knopf and Koop*, 2006]. Prior water uptake and immersion freezing experiments did not have a significant effect on deposition ice nucleation within experimental uncertainty. The ice nucleation data of both deposition ice nucleation experiments, conducted before and after the water uptake and immersion freezing experiments, were used for analysis.

3. Results and Discussions

[18] Applying the binomial distribution, we can estimate the minimum particle sample size to obtain a representative subset (i.e. identified particle-type classes as defined below) of the entire particle population with a given confidence interval and margin of error (ME) according to *Levy and Lemeshow* [1991]

$$N = \frac{z^2 \times p \times (1-p)}{M E^2}, \quad (1)$$

where z is the tabulated z-value of the normal distribution (i.e. 2.33 for 99% confidence interval) and p is the probability of a particle belonging into a particle-type class. This approach strictly holds only if the particle population is

made of two particle-type classes. Applying the minimum and maximum numbers of particles sampled (368 and 7602; see Table 1) and assuming a particle-type class into which 50% of identified particles belong, we obtain that sampled particles are representative of the entire population with 99% confidence and a ME of 6.1% and 1.3%, respectively. ME will be lower for smaller or larger particle classes and for a smaller confidence interval, i.e. 95%. When deriving the minimum particle sample size for a population made of arbitrary numbers of particle-type classes following *Thompson* [1987], we obtain that sampled particles are representative of the entire population with 99% confidence and a ME of 7.3% and 1.6%, respectively. Thus, the presence of multiple particle-type classes within the particle population either slightly increases minimum particle sample size or corresponding ME. The same values of the confidence level and ME are applicable for the particle populations deposited on different substrates installed on the same rotating impaction plate of MOUDI. In this sampling approach particles are distributed evenly over a wide deposition area which is larger than an individual substrate by factor of ~25 (see Figure S1). This sampling procedure ensures that all employed substrates are exposed to the same ambient particle population. Therefore, using different substrates for chemical analyses and ice nucleation experiments should result in comparable results.

[19] Majority of the ice nucleation events (>90% out of 330) occurred on particles larger than 200 nm which was visually confirmed by the recorded images. Thus, the unidentified particles (<200 nm) in the investigated samples do not contribute a significant fraction of ice nucleation events. During CCSEM/EDX and STXM/NEXAFS analyses, the particle samples were exposed to vacuum and 1 atm of helium conditions, respectively. Thus, volatilization of volatile organic material cannot be ruled out. However, over the course of these experiments no size change of the organic particles was detected. This strongly suggests that the organic phase was in a highly viscous or glassy state.

[20] In repeated deposition ice nucleation experiments with the same sample at the same temperature, we observed different particles nucleating ice in the vast majority of the experiments. For the CalNex samples, about 85% of the deposition ice nucleation events (~160 in total) occurred on different IN. This is in striking contrast to our previous studies of ice nucleation on laboratory standards of mineral dust particles. In those experiments, repeated ice nucleation events were recorded on the same most efficient IN [*Knopf and Koop*, 2006; *Wang and Knopf*, 2011].

[21] In this study exact chemical composition of the individual ice nucleus could not be experimentally determined. Instead, we make an effort to correlate the observed trends in water uptake and ice nucleation with the trends in chemical composition derived from single-particle analysis data. Nevertheless, with these caveats our results show onsets for water uptake and ice nucleation relevant to air parcels containing particles similar to the ones sampled in the field allowing assessment of the importance of such particles for atmospheric glaciation processes. The mean onset conditions of ice nucleation and water uptake by particles are discussed in the remaining text. The range of onset conditions are provided.

3.1. Particle Morphology, Coating, Mixing State, and Chemical Composition

3.1.1. Particle Morphology, Coating, and Elemental Composition Determined by CCSEM/EDX Analysis

[22] Table 1 summarizes the sample characteristics such as particle number density on the substrate and mean particle sizes as determined by CCSEM/EDX analysis for the investigated samples [*Laskin et al.*, 2003, 2006; *Knopf et al.*, 2010]. The mean diameters are defined as the equivalent circle diameters of the 2-D projected area of particles from the microscopy images. The mean particle diameter ranged from 0.26 to 0.52 μm. The particle number density ranged from 0.2×10^6 to 2.3×10^6 mm^{-2}. Combining the particle number density, mean diameter, and the sample area observed in the ice nucleation experiments, the particle surface area available for ice nucleation was determined as 0.05×10^{-2} to 0.26×10^{-2} cm^{-2}. This value may represent a lower limit of the actual particle surface area due to the non-spherical geometry of the particles and the fraction of undetected small particles (<200 nm) by the CCSEM/EDX analysis.

[23] Typical SEM images of the particle samples investigated in this study are shown in Figure 1. Soot particles identified by STXM/NEXAFS, which primarily are produced during combustion processes, are less transparent to the electron beam in Scanning Transmitted Electron Microscopy (STEM) imaging mode of SEM and thus appear darker than the remaining organic material (see images of the A2, A3, and A4 samples). Higher atomic number elements, such as sulfur as identified by the CCSEM/EDX analysis, most likely present as sulfate, are also less transparent in the STEM images as compared to their thin organic coatings (see images of the B2 and B4 samples). More particles of A3 sample contained soot/inorganic inclusions than A2 and A4 samples. Particles of A2 and A4 samples showed near spherical shapes whereas particles of A3 sample were non-spherical. M1 sample collected from the MILAGRO campaign exhibited non-spherical, needle-like shapes. Particle samples collected during the CalNex campaign exhibited visible organic coatings of various thicknesses for the majority of the particles.

[24] The sizes of soot/inorganic cores and thickness of the organic coatings were estimated from STEM images acquired at different brightness and contrast settings. Representative STEM images recorded for these estimates are shown in Figure S4 in the auxiliary material. First, the brightness and contrast settings were tuned to obtain the contours of the entire particles and then corresponding particle sizes were recorded. Then, the settings were changed to make only inclusions visible, and their sizes were also recorded. The thickness of organic coatings was then estimated from the size differences between whole particles and their inclusions. Using this approach, we estimated the thickness of organic coatings using the mean sizes of particles and their inclusions. For example, for B4 sample, particles and their inclusions with a mean diameter of ~0.26 and 0.22 μm, respectively, were determined from analysis of ~530 particles. The organic coatings of particles in B4 sample is therefore ~0.04 μm. Organic coatings are estimated to be from 0.04 to 0.13 μm, where B4 sample exhibits thinnest and A3 thickest coatings. Incomplete coverage for the cases of thin organic coatings cannot be ruled out. It should be noted that these estimates

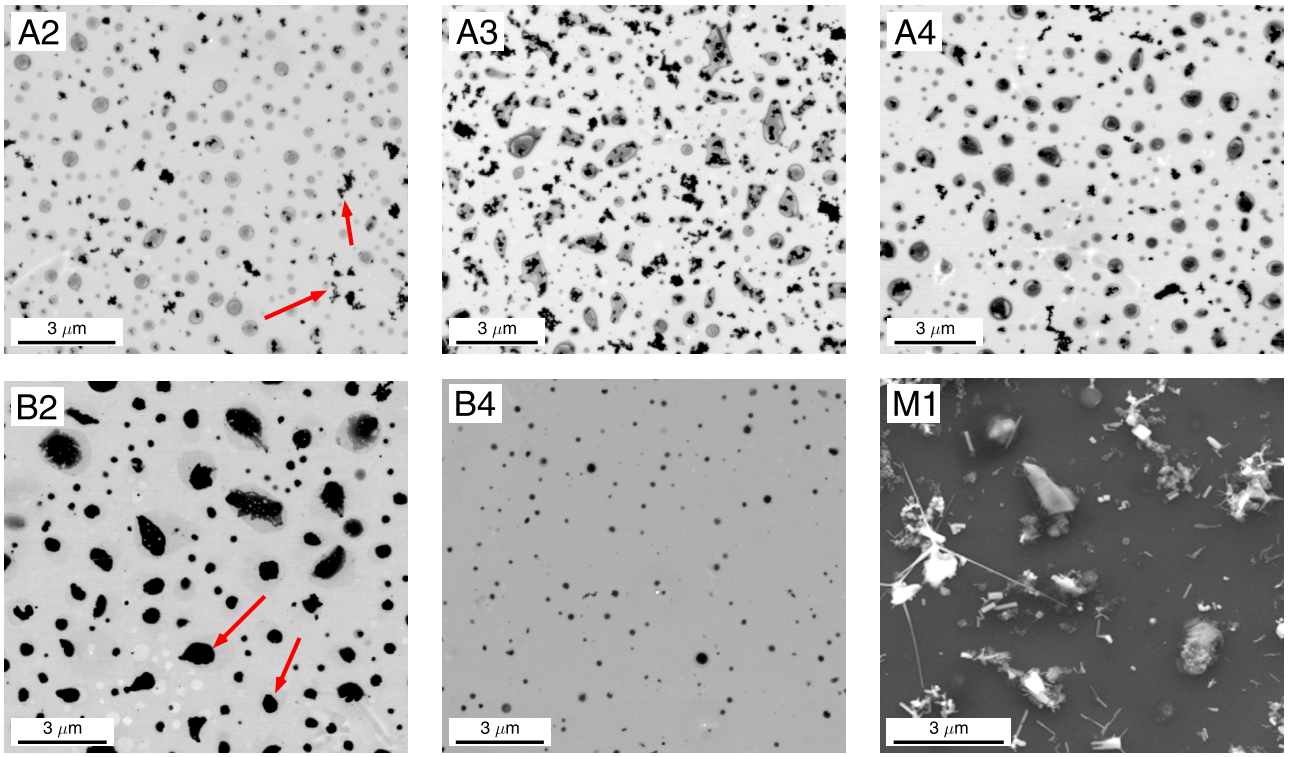

Figure 1. Typical scanning electron microscopy (SEM) images obtained by using STEM (Scanning Transmitted Electron Microscopy) detector for aerosol particles of the A2, A3, A4, B2, and B4 samples collected during the CalNex campaign, and a SEM image obtained by using secondary electrons detection for the M1 sample collected during MILAGRO campaign. Typical soot particles are indicated by arrows in the image for A2 sample and sulfate particles are indicated in the image for B2 sample.

represent rough values. The coatings of particles on A2, A3, and A4 samples are in general thicker than for particles on B2 and B4 samples. *Veres et al.* [2011] found that an increase in concentrations of gas phase organic acids at the ground site when air resided long time periods in the L.A. basin encountered on May 31 to June 6. This study suggested that the dominant source of these organic acids which correlated well with HNO_3 and O_X measurements was photochemical production from urban emissions. This indicates that on May 19 the air mass most likely underwent strong photochemical processes since wind speeds were low. Whereas for May 23, the concentrations of the organic acids were significantly lower [*Veres et al.*, 2011] yielding weaker photochemical processes. Thus, the thicker carbonaceous coating and higher fraction of pure organic particles present in A samples were most likely due to the enhanced photochemical processes and formation of SOA compared to B samples.

[25] CCSEM/EDX analysis provides the elemental composition for a significant number of individual particles ranging from ~2100 to 7600 particles for A2, A3, A4, B2, and B4 particle samples. Particles were classified into four classes as follows: (1) CNO, in which particles mainly contain C, O, and occasionally traces of N, indicates carbonaceous particles without explicit distinguishing of soot (black carbon) from organic particles; (2) CNOS, in which particles contain C, N, O, S, and occasionally traces of K, represents sulfates or other sulfur containing particles including their internal mixtures with either organics or soot; (3) Na/Mg rich, in which particles contain Na or Mg with the total atomic percent of Na and Mg higher than the total atomic percent of other detected metals, represents particles of marine origin; (4) the rest of the particles that don't fall in previous classification were included in the "Other" particle-type class. The relative abundance of each class is shown in Figure 2a. The maximum relative error for presented particle-type class percentages determined by CCSEM/EDX is 10% for the first three classes. The relative error for class "Other" ranges from 6–24% due to the significant smaller particle number assigned to this class. Majority of the particles in A2 and A3 samples were CNO type which could be organic material or soot particles. During the course of the day of May 19, the number fraction of CNOS class in A2, A3, and A4 samples increases from 19, 33, to 54%, respectively. This could be due to the condensation of sulfates on the particles [*Johnson et al.*, 2005]. A3 sample exhibited a higher number fraction of Fe-containing particles (3%) which were included in the category "Other" (6%) compared to the other samples. 73 and 53% of the particles present in B2 and B4 samples contained sulfur, respectively, whereas Na/Mg rich particles which are indicative of sea salt contributed ~21% of particles. The number fraction of Na and Mg containing particles was enhanced in B2 and B4 samples compared to A2 and A3 samples. The number fraction of Mg-containing particles present in B2 sample (10%) was especially high compared to <1% for A2 and A3 samples. Overall, the CCSEM/EDX analysis indicated that A2 and A3 samples mainly contain soot associated with organic material

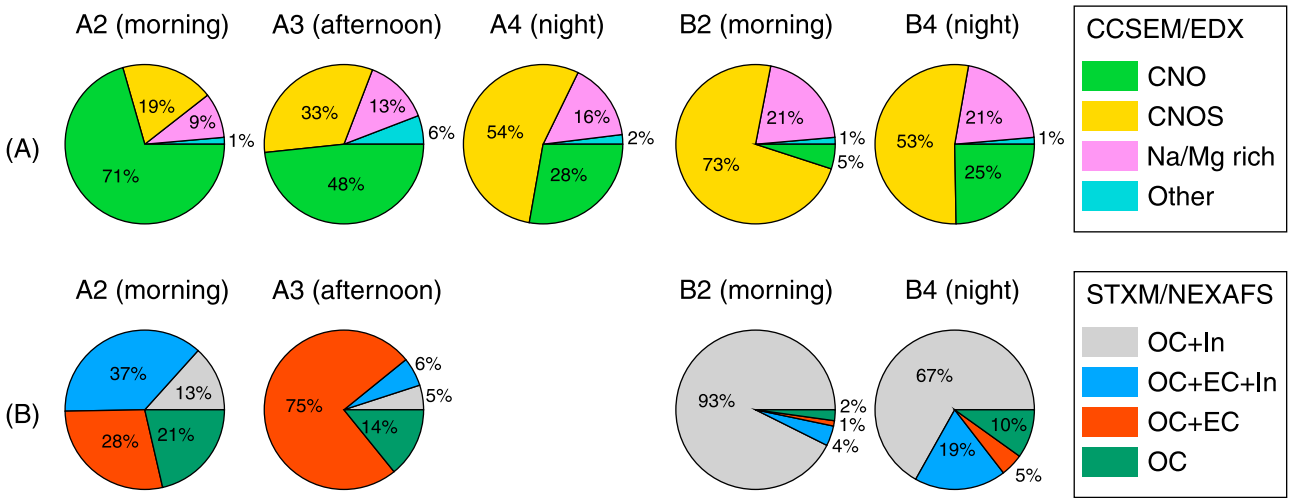

Figure 2. The percentage number fraction of identified particle-types classes for each sample as classified by (a) CCSEM/EDX and (b) STXM/NEXAFS. See text for more details.

whereas B2 and B4 samples were dominated by sulfate and sea salt indicating the influence of marine sources.

3.1.2. Particle Mixing State and Chemical Composition Determined by STXM/NEXAFS Analysis

[26] STXM/NEXAFS provides speciation of the carbonaceous content of individual particles and the mixing state of aerosol particles for A2, A3, B2, and B4 samples. Particles were classified according to 4 categories: (1) OC: particles are mainly carbonaceous; (2) OC+EC: soot with organic coatings; (3) OC+EC+In: particles are coated with organics and have soot and inorganic inclusions; (4) OC+In: Inorganic particles most of which have a thin organic coating. STXM/NEXAFS analysis of a statistically significant number of identified particles (up to 760) shows that the majority of particles from A2 (morning), A3 (afternoon), B2 (morning), and B4 (nighttime) samples possess an organic coating. The percentage number fraction of the different particle types for each sample is shown in Figure 2b. STXM/NEXAFS analysis of particles indicated that A2 and A3 samples consisted of particles which were internally and externally mixed with soot/inorganic and organic material whereas the majority of the particles on the B2 and B4 samples contained a mixture of inorganic and organic material. A total of ~65% of the particles present in A2 sample were classified as soot with organics (OC+EC) or soot with inorganics and organics (OC+EC+In). Similarly, about 80% of the particles present in A3 sample fall into these two categories. The presence of soot indicates that A2 and A3 samples were affected by anthropogenic sources, such as traffic related emissions. In addition, A3 sample has more carboxylic groups associated with particles compared to A2 sample as determined by the STXM/NEXAFS analysis. This increase can likely be contributed to heterogeneous oxidation of soot particles by atmospheric trace gases such as O_3, NO_3, and OH during the day [*Akhter et al.*, 1985; *Smith et al.*, 1988; *Chughtai et al.*, 1991; *Daly and Horn*, 2009]. B2 and B4 samples were dominated by inorganic particles with thin coatings of organic material. These particles contribute to 93% and 67% of the total particle number, respectively. B4 sample contained more particles with soot inclusions and more purely organic particles compared to B2 sample as shown in Figure 2b. B2 and B4 samples were much less carbonaceous than A2 and A3 samples. More detailed particle characterization of A2, A3, B2, and B4 samples will be presented in a separate manuscript by A. Laskin et al. (manuscript in preparation, 2012).

[27] Sample M1 was dominated by internally mixed particles consisting of Pb/Zn chlorides and nitrates [*Moffet et al.*, 2008]. These Pb/Zn-containing particles represented the majority of the fine mode particles as determined by aerosol time-of-flight mass spectrometer (ATOFMS), CCSEM/EDX, and STXM/NEXAFS [*Moffet et al.*, 2008]. Sample M1 was collected after a period of heavy rainfall when background aerosol concentration was low. During the period of interest, Pb/Zn-containing particles accounted for 61% as detected by ATOFMS and 73% as determined by CCSEM/EDX. These particles were typically mixed with soot, indicating a combustion source, and their chemical compositions closely match signatures indicative of waste incineration [*Moffet et al.*, 2008]. *Moffet et al.* [2008] concluded that many Zn-rich particles composed of $Zn(NO_3)_2{\cdot}6H_2O$ and ZnO possess needle-like structures, similar to those shown in Figure 1. For these reasons, this sample was chosen for ice nucleation measurements of particles representative of waste incineration [*Moffet et al.*, 2008].

[28] Particle chemical composition, as determined by CCSEM/EDX and STXM/NEXAFS analyses, indicates that A2, A3, and A4 samples were mainly affected by anthropogenic sources whereas B2 and B4 samples were significantly influenced by marine sources. Sample M1 consisted of Pb/Zn-containing inorganic particles which are apportioned to anthropogenic emissions relevant to waste incineration [*Moffet et al.*, 2008]. More detailed descriptions on the particle characteristics of A2, A3, B2, B4, and M1 samples are given by *Moffet et al.* [2008] and Laskin et al. (manuscript in preparation, 2012).

3.2. Onset Conditions of Water Uptake and Immersion Freezing

3.2.1. CalNex Samples: A2, A3, and A4 Collected on May 19

[29] The range and mean onset conditions of immersion freezing and water uptake by the investigated samples were

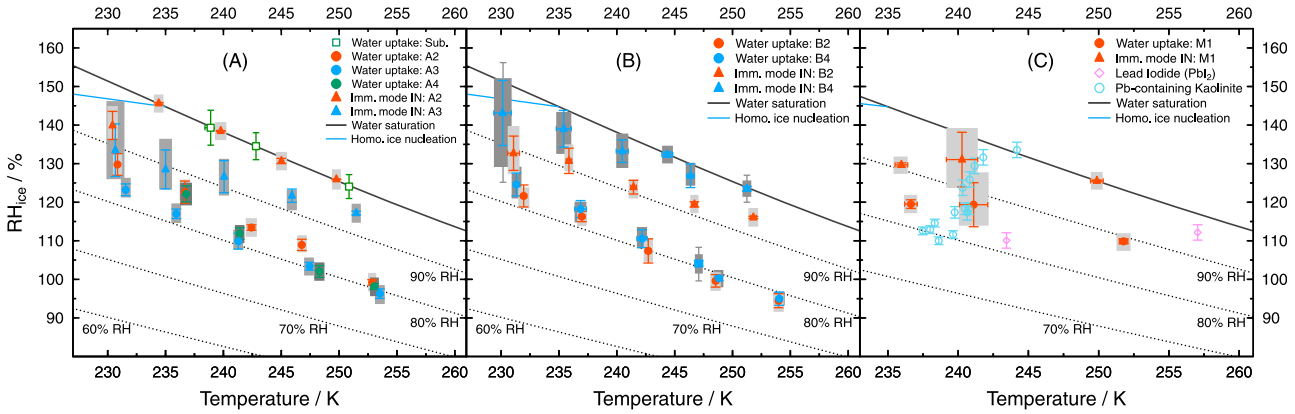

Figure 3. The mean onset conditions for ice nucleation via immersion freezing (solid triangles) and water uptake (solid circles) as a function of temperature and RH_{ice}. The range of onset conditions are shown as bars with different gray levels indicating the corresponding samples. (a) A2, A3, and A4 particle samples collected on May 19 are indicated in red, blue, and green, respectively. (b) B2 and B4 particle samples collected on May 23 are indicated in red and blue, respectively. (c) M1 particle sample is indicated in red; ice nucleation by lead iodide (PbI_2) [*Detwiler and Bernard*, 1981] and Pb-containing kaolinite [*Cziczo et al.*, 2009] are shown as open diamonds and circles, respectively. The onset condition for water condensation on blank substrates are shown in green squares in Figure 3a. Error bars indicate one standard deviation. Representative maximum experimental uncertainties are given in Figure 3b for the selected temperatures. The black solid line indicates water saturation (100% *RH*). The diagonal dotted lines (top right to bottom left) indicate 90%, 80%, 70%, and 60% *RH*. The blue solid line represents the RH_{ice} thresholds for homogeneous ice nucleation of an aqueous droplet with 0.3 μm in diameter corresponding to a homogeneous ice nucleation rate coefficient of about 1.2×10^{12} cm^{-3} s^{-1} [*Koop et al.*, 2000a].

determined as a function of T_p and RH_{ice} as presented in Figure 3. The corresponding RH_{ice} for constant *RH* values of 60, 70, 80, and 90% are also shown. Figure 3a shows that water uptake by A3 and A4 samples occurred between 79 and 86% *RH* for temperatures between 272 K and 231 K, respectively. A2 sample took up water at slightly higher *RH* of 81–87%. This demonstrates that in average the particles of A3 sample were more hydrophilic than the ones of A2 sample. This may be due to the increased number of carboxylic groups present on particles of A3 sample as compared to A2 sample, but effects are not well documented in the literature and more studies are needed. For the particles collected during the CalNex campaign the mean *RH* onsets for water uptake increase 3–6% as the particle temperature decreases by 22–35 K. For example, the *RH* onsets of water uptake for A4 sample increase from ~80 to 86% within 35 K when particle temperatures decrease from 272 to 237 K.

[30] Above 230 K, ice nucleation occurred after water uptake via immersion freezing at *RH* of 91–100% and 84–95% for A2 and A3 samples, respectively. Water uptake by A4 sample was observed at *RH* values similar to A3 sample but ice formation was not observed before reaching water saturation. A3 sample showed significant higher ice nucleation efficiencies via immersion freezing (at water subsaturated conditions) than A2 sample.

3.2.2. CalNex Samples: B2 and B4 Collected on May 23

[31] Figure 3b shows that B2 and B4 samples first took up water at 77–86% *RH* in the temperature range of 230–275 K, and then induced immersion freezing when *RH* was further increased. The *RH* onsets for water uptake increase by 3–6% as particle temperatures decrease by about 22 K for both B2 and B4 samples. These results are similar to *Adachi et al.* [2011], who used a TEM to show that sulfate-containing particles collected on May 30, June 13, and June 15 during the CalNex campaign deliquesced at (80±4)% *RH* at 298.15 K. This is similar to onset *RH* values for water uptake by the particles of B2 sample which contain a large amount of sulfur as determined by CCSEM/EDX analysis. Above 230 K, Figure 3b demonstrates that B2 sample induced immersion freezing at *RH* values of 85–94%, i.e., in the water subsaturated regime, after water uptake. B4 sample induced immersion freezing at *RH* values of 89–100%.

3.2.3. M1 Sample Collected During the MILAGRO Campaign

[32] The ice nucleation efficiency of M1 sample which consisted of a major fraction of Pb/Zn-containing particles was also examined. Figure 3c shows that above 231 K water uptake by the particles was observed at 84–89% *RH* and was followed by immersion freezing at 90–100% *RH*. M1 sample behaved significantly different with regard to water uptake and immersion freezing compared to the samples collected during the CalNex campaign. For comparison, the onset conditions of ice nucleation by lead iodide (PbI_2) [*Detwiler and Bernard*, 1981] and Pb-containing kaolinite [*Cziczo et al.*, 2009] are shown in Figure 3c. *Cziczo et al.* [2009] have shown that Pb-containing kaolinite particles can serve as efficient IN at temperatures between 235 K and 245 K. An early study by *Detwiler and Bernard* [1981] showed that PbI_2 particles, which were applied in cloud seeding, also exhibited high ice nucleation efficiencies. Previous studies have shown that ZnO particles could also serve as IN at 253 K and 263 K [*Gorbunov and Safatov*, 1994]. The Pb/Zn chlorides and nitrates are soluble in water whereas ZnO is insoluble, thus it would be expected that after water uptake

by the soluble material, the insoluble components present in M1 sample, such as ZnO, may have served as immersion freezing IN. In summary, this work is in good agreement or supports the work of others that have shown Pb/Zn-containing particles may act as efficient IN in the immersion freezing mode.

3.2.4. Effects of Chemical Composition on Water Uptake and Immersion Freezing

[33] For temperatures above 231 K, the averaged chemical composition of the CalNex particles influenced by anthropogenic and marine sources is reflected in the general trends in water uptake and immersion freezing efficiencies. As will be outlined below the particles nucleating ice belong with very high confidence to the identified particle-type classes. Figure 1 shows that the samples are visually different and this is reflected in the particle-type class distributions given in Figure 2. All particle-type classes are present on each sample in significant numbers but observed water uptake and ice nucleation onsets differ from sample to sample. The dominant fraction of the particle-type class changes from sample to sample and from day to day. For example, B samples contained much more inorganic particles compare to A samples as shown in Figure 2. For these reasons we relate the change in the dominant fraction of the particles to observed changes in the onsets of water uptake and ice nucleation. In other words we relate trends in particle composition and mixing state changes with changes in water uptake and ice nucleation onsets. Although trends in water uptake and ice nucleation onsets follow to a first order expected trends in particle composition and mixing state, the effect of a minor particle fraction on water uptake and ice nucleation onsets could be masked by this approach.

[34] A3 sample took up water at lower RH than A2 sample may be due to the enhancement of carboxylic function groups. A3 and A4 samples may contain similar hydrophilic carboxylic groups due to the photochemical aging processes during the day and thus, exhibit similar water uptake. Although, B4 sample contained more particles with soot inclusions and more purely organic particles compared to B2 sample, these two samples exhibited similar water uptake. Figure S5 also shows the deliquescence relative humidity (DRH) of ammonium sulfate and NaCl below 275 K for comparison [*Onasch et al.*, 1999; *Cziczo and Abbatt*, 2000; *Koop et al.*, 2000b; *Braban et al.*, 2001; *Parsons et al.*, 2004]. The DRH of ammonium sulfate increases from ~80 to 86% whereas DRH of NaCl increases from ~75 to 80% as temperature decreases from 275 to 235 K. B2 and B4 samples exhibited a similar temperature dependency compared to ammonium sulfate and NaCl particles.

[35] Immersion freezing is triggered by the insoluble components of the particles. Thus, the insoluble cores play an important role in determining immersion freezing efficiencies of the particles. The differences in immersion freezing onsets among the investigated particle samples was most likely due to the differences in the insoluble inclusions. Although the efficiency of soot particles serving as IN remains unclear [e.g., *DeMott*, 1990; *Gorbunov et al.*, 2001; *Möhler et al.*, 2005; *Dymarska et al.*, 2006; *Cozic et al.*, 2008], several studies have shown that soot particles could act as IN [e.g., *Diehl and Mitra*, 1998; *Popovicheva et al.*, 2008; *Fornea et al.*, 2009; *Koehler et al.*, 2009]. The soot inclusions present in the investigated particle samples may have served as IN after water uptake. The particles with an enhanced number of carboxylic groups may contribute to the higher immersion freezing efficiency of A3 sample compared to A2 sample since the carboxylic groups may provide more hydrogen bonding sites to attract water molecules [*Pruppacher and Klett*, 1997; *Knopf and Forrester*, 2011]. The number fraction of particles containing metals including Fe, Zn, Ca and Al elements, is ~6% for A3 sample compared to ~1% for A2 sample as determined by CCSEM/EDX analysis. In particular, the Fe-containing particles account for 3% of A3 samples compared to 0.6% for A2 sample. This indicates that A3 sample may consist of mineral dust inclusions which could also result in the corresponding higher immersion freezing efficiencies. The B2 morning sample influenced by marine source showed a higher propensity to form ice via immersion freezing compared to A2 morning sample affected by anthropogenic sources as shown in Figures 3a and 3b.

3.3. Onset Conditions for Deposition Ice Nucleation

3.3.1. CalNex Samples: A2, A3, and A4 Collected on May 19

[36] The range and mean onset conditions of deposition ice nucleation by the investigated samples were determined as a function of T_p and RH_{ice} as presented in Figure 4. The substrates nucleated ice close to RH_{ice} thresholds of homogeneous ice nucleation. This could be due to water condensation on small defects of the hydrophobic substrate, which can't be detected by optical microscope, followed by homogeneous ice nucleation once corresponding RH_{ice} thresholds are reached. Figure 4a demonstrates that below 230 K A2, A4, and A3 samples nucleated ice via deposition mode at mean RH_{ice} values of 134–150% which are well below water saturation and are ~10 to 20% lower than the homogeneous freezing limits [*Koop et al.*, 2000a]. A3 sample exhibited lower mean RH_{ice} onsets for deposition ice nucleation than A2 sample except at 220 K. However, those differences lie within the experimental uncertainties. Student's T-test shows that the differences in mean RH_{ice} values for A2 and A3 samples over the observed temperature range are not statistically significant.

3.3.2. CalNex Samples: B2 and B4 Collected on May 23

[37] B2 and B4 samples nucleated ice at mean RH_{ice} values from 123 to 142% via deposition mode below 230 K which are ~10–35% lower than the homogeneous freezing limits [*Koop et al.*, 2000a] as shown in Figure 4b.The RH_{ice} onset values for B4 sample (nighttime) are in average ~2–5% RH_{ice} higher than B2 sample (morning). However, within the experimental uncertainties, B2 and B4 samples exhibited similar deposition ice nucleation efficiencies. The data demonstrate that B2 and B4 samples were very efficient ice nuclei which can induce deposition ice nucleation at RH_{ice} as low as 120% for the investigated temperature range. When comparing deposition ice nucleation onsets of A and B samples, the inorganic-containing particles present in A samples may have not contributed to the observed ice nucleation due to the present of thick organic coatings as discussed above, otherwise A samples may have nucleated ice at RH_{ice} similar to B samples having thinner and/or incomplete organic coatings. In general, below 220 K, the marine influenced samples (B2 and B4) exhibited a higher propensity to form ice via

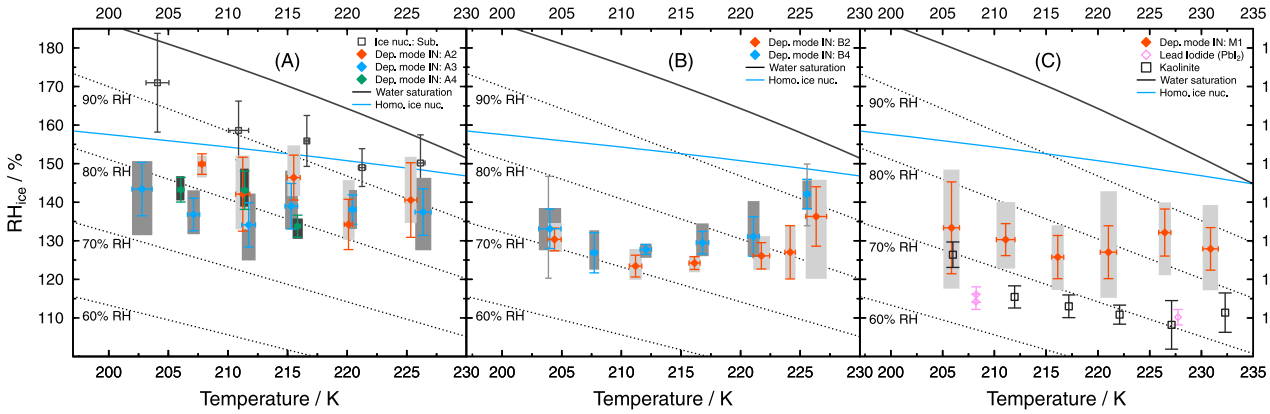

Figure 4. The mean onset conditions for deposition ice nucleation as a function of temperature and RH_{ice}. The range of onset conditions are shown as bars with different gray levels indicating the corresponding samples. (a) A2, A3, and A4 particle samples are indicated in red, blue, and green, respectively. (b) B2 and B4 particle samples are indicated in red and blue, respectively. (c) M1 particle sample is indicated in red; ice nucleation by lead iodide (PbI_2) [*Detwiler and Bernard*, 1981] and kaolinite [*Knopf et al.*, 2010] are shown as open diamonds and squares, respectively. The onset conditions for deposition ice nucleation on blank substrates are shown in open squares in Figure 4a. Error bars indicate one standard deviation. Representative experimental uncertainties are given in Figure 4b for the selected temperatures. The remaining lines are identical to those in Figure 3.

deposition mode than the samples containing anthropogenic organics (A2, A3 and A4).

3.3.3. M1 Sample Collected During the MILAGRO Campaign

[38] Below 231 K, M1 sample nucleated ice via deposition mode at mean RH_{ice} onset values of 126–133% as shown in Figure 4c. The onset conditions of ice nucleation by lead iodide (PbI_2) [*Detwiler and Bernard*, 1981] and kaolinite [*Knopf et al.*, 2010] are also shown for comparison. Below 210 K, M1 sample exhibited high ice nucleation efficiencies that are comparable to kaolinite particles. *Detwiler and Bernard* [1981] showed that PbI_2 particles exhibited high ice nucleation efficiencies similar to kaolinite particles.

3.3.4. Effects of Particle Morphology and Chemical Composition on Deposition Ice Nucleation

[39] We make an effort to correlate observed trends in ice nucleation onsets at low temperature with the overall variability in particle composition and morphology as inferred from the major particle-type classes. The reasons for this approach are outlined below. The number of individual particles present in a field-of-view of the optical microscope during ice nucleation experiment is in the order of one million. As mentioned above, in repeated experiments deposition ice nucleation occurred on different particles for the same sample at the same temperatures. These observations, as well as the repeatable RH_{ice} values at which ice nucleation onsets were recorded in each of the samples, suggest that it is unlikely that ice nucleation events took place on some exceptionally unique particles which might have superior propensity for ice nucleation (e.g. such as those of kaolinite, for instance). Therefore, we make the assumption that likely particles from common classes may exhibit sufficient propensity to serve as IN observed in our experiments. Based on this hypothesis, we assume that all the particles possess the same ice nucleation ability to infer the plausibility that the occasional outliner particles from "Other" group, may have nucleated ice. Applying the law of total probability and Bayes' theorem [*Lee*, 2004] it can be shown that the probability, p, of an observed ice nucleation event being initiated by particles from the "Other" group is 1% . Applying the same analysis but assigning the "Other" particles a 10 and 100 times higher ice nucleation efficiency will result in a p = 9.2 and 50% for an ice nucleation event being initiated by "Other" particles. The probability that n IN stem from "Other" is therefore p^n. However, if "Other" nucleate ice 10–100 times more efficient, one would assume to see a trend to lower onset RH_{ice} values when the particle number of "Other" increased by a factor of 6 (e.g. difference in relative contribution of "Other" between samples A2 and A3). However, this is not the case. Moreover, if the "Other" particle class contains efficient IN properties similar to mineral dust, and taking into account available surface areas of these particles, lower ice nucleation onsets should have been observed as given in Table 2. Also, for temperatures above 230 K the field-collected particles always take up water first and then in some cases freeze via immersion mode below water saturation. In contrast, calcite and quartz minerals nucleate ice via deposition mode at 235 K [*Eastwood et al.*, 2008] and kaolinite particles nucleate ice via deposition mode between 235 and 250 K [*Wang and Knopf*, 2011]. From this we infer that it is plausible that major identified particle-type classes might be responsible for the observed ice nucleation and that the likelihood that observed trends in water uptake and ice nucleation are governed by a minor particle fraction of the collected sample may be very small.

[40] No water uptake was observed prior to deposition ice nucleation below 230 K for all investigated particle samples. The chemical and physical characteristics of particle surfaces, such as chemical functional groups, hygroscopicity, and morphology, determine corresponding deposition ice nucleation efficiencies [*Pruppacher and Klett*, 1997; *Wang and Knopf*, 2011]. As discussed above, A3 sample possessed more carboxylic functional groups but did not exhibit significantly different deposition ice nucleation efficiencies

Table 2. The Ranges of Mean RH_{ice} Onsets for Deposition Ice Nucleation by Ambient Particles Collected in Los Angeles (A Samples) and in/Around Mexico City, the Amorphous SOA, Unoxidized SRFA, O_3-Oxidized SRFA Particles, and Various Types of Mineral Dust[a]

Particle Type	Temperature (K)	RH_{ice}[b] (%)	Particle Size (μm)	Surface Area ($\times 10^{-2}$ mm^2)	References
Los Angeles (A2)	200–230	(134–150) ± 10	0.32 ± 0.1	26 ± 4	this study
Los Angeles (A3)	200–230	(134–143) ± 7	0.37 ± 0.1	24 ± 4	this study
Los Angeles (A4)	200–230	(133–143) ± 5	0.39 ± 0.1	24 ± 4	this study
SOA High O/C	200–230	(141–149) ± 14	0.7 ± 0.7	1.1 ± 0.3	*Wang et al.* [2012]
SOA Medium O/C	200–230	(139–152) ± 11	1.1 ± 1	5.4 ± 1.4	*Wang et al.* [2012]
SOA Low O/C	200–230	(136–146) ± 7	0.7 ± 0.8	3.0 ± 0.8	*Wang et al.* [2012]
Mexico City (In)	200–231	(122–138) ± 9	0.4–0.7	4.8–8.0	*Knopf et al.* [2010]
Mexico City (Around)	200–231	(124–137) ± 7	0.5–0.7	6.6–8.1	*Knopf et al.* [2010]
Unexposed SRFA	200–241	(133–148) ± 8	(2.0–2.4) ± 1.0	1.4–3.8	*Wang and Knopf* [2011]
O_3–exposed SRFA	200–241	(133–147) ± 9	(2.4–2.9) ± 1.4	2.0–7.3	*Wang and Knopf* [2011]
Kaolinite	200–255	(105–121) ± 5	(2.3–4.3) ± 2.0	1.3–7.9	*Wang and Knopf* [2011]
Kaolinite	218–243	(107–129) ± 8	0.1–0.8	6.3–400[c]	*Welti et al.* [2009]
Kaolinite	236–246	(104–105) ± 5	~7.7	0.5–2.4	*Eastwood et al.* [2008]
Saharan dust	233	(102–115) ± 4	0.5–5	0.9–320	*Kanji and Abbatt* [2006]
Arizona test dust	233	(103–120) ± 5	0.5–5	30–300	*Kanji et al.* [2008]
Arizona test dust	223	(105–160) ± 5	0.04–0.24	0.3–100[d]	*Kanji and Abbatt* [2010]
Arizona test dust	218–243	(105–135) ± 4	0.1–0.8	6.3–400[c]	*Welti et al.* [2009]
Montmorillonite	236–245	(106–124) ± 5	~8.1	1.1–2.2	*Eastwood et al.* [2008]
Montmorillonite	218–243	(106–121) ± 4	0.1–0.8	6.3–400[c]	*Welti et al.* [2009]
Muscovite	237–246	(102–107) ± 6	~9.0	0.5–2.0	*Eastwood et al.* [2008]
Illite	218–243	(105–128) ± 4	0.1–0.8	6.3–400[c]	*Welti et al.* [2009]
Quartz	234–244	(136–137) ± 4	~10.0	2.1–2.9	*Eastwood et al.* [2008]
Calcite	234–244	(132–135) ± 6	~14.2	1.6–7.7	*Eastwood et al.* [2008]

[a]Adapted from *Wang et al.* [2012]. The investigated temperature ranges, mean particle size, and total particulate surface area available for ice nucleation are also given.

[b]Mean RH_{ice} onsets for the investigated temperature range with maximum one standard deviation.

[c]The experiments were conducted using Zürich Ice Nucleation Chamber [*Welti et al.*, 2009]. Typical aerosol number concentrations were 1000 particles per cm^3 (N). The total air flow through the chamber was 10 liters per minute (V). Within the 12 s residence time (t), the total particulate surface area in the chamber is estimated by $SA = \pi D^2 NVt$. D is particle size in diameter.

[d]The experiments were conducted using continuous flow diffusion chamber [*Kanji and Abbatt*, 2010]. Typical aerosol number concentrations were 500–1000 particles per cm^3. The total air flow through the chamber was 2.8 liters per minute. Within the 12 s residence time, the total particulate surface area in the chamber is estimated using same method as given in footnote b.

than A2 sample. Thus, the abundance of carboxylic groups on particles due to photochemical aging may have a minor effect on deposition ice nucleation. Previously, a similar effect was observed and it was concluded that additional organic coating (SOA) due to photochemical processing does not strongly affect deposition ice nucleation of organic-dominated particles [*Knopf et al.*, 2010]. The reason for this observed effect may be related to the formation of an amorphous solid phase of the organic material yielding active sites to nucleate ice at low temperatures typical for deposition nucleation [*Murray et al.*, 2010; *Virtanen et al.*, 2010; *Zobrist et al.*, 2011; *Koopet al.*, 2011; *Wang et al.*, 2012].

[41] Our assumption that organic material governs observed ice nucleation onsets of A samples might be indirectly inferred. The change of IN in repeated experiments and slight variation in the RH_{ice} onset values in each experimental run suggests that most likely particles experience morphological changes when the organic material transfers from glassy to liquid state and vice versa when repeating the experiments. *Mikhailov et al.* [2009] have shown that shape and porosity of amorphous and crystalline particles depend on chemical composition and drying conditions. These observations are in contrast to the behavior of mineral dust particles. Furthermore, the organic dominated A2 sample initiates water uptake, immersion freezing, and deposition ice nucleation at similar onsets as laboratory generated SOA particles with similar bulk oxidation level [*Wang et al.*, 2012]. Our results indicate that water uptake and deposition ice nucleation by the organic dominated particles in A2 sample are also in agreement with derived SOA glass transition curve [*Wang et al.*, 2012]. Assuming that the same glass transition characteristics are applicable for particles in sample A, we see that water uptake was observed when particles were in the semi-solid or liquid phase, whereas particles in the solid (glassy) phase nucleated ice via deposition mode. This reported correlation is not achieved by any other previously investigated organic and inorganic particle types [*Knopf et al.*, 2010; *Wang et al.*, 2012]. Furthermore, it has been previously shown that organic containing particles can be efficient IN [*Baustian et al.*, 2012] and that monocarboxylic acids [*Schill and Tolbert*, 2012] induce deposition ice nucleation similar to SOA coated ambient particles collected in Mexico City [*Knopf et al.*, 2010]. A separate study by *Chou et al.* [2012] reports that soot particles coated with oxidation products of α-pinene resulted in enhanced freezing efficiencies. With less or thinner organic coatings present, the inclusions may affect deposition ice nucleation as indicated by the contrasting ice nucleation efficiencies between B2 and B4 samples and A2 and A3 samples.

[42] Organic coating on the particles collected during the CalNex campaign may be in an amorphous solid state at freezing temperatures [*Zobrist et al.*, 2008, 2011; *Koop et al.*, 2011]. These potentially amorphous solid particle surfaces of A2, A3, and A4 samples may provide a sufficient and similar number of active sites to initiate deposition ice nucleation at similar RH_{ice} onsets. A similar argument applies to the deposition ice nucleation efficiencies for B2 and B4

samples which contain more inorganic inclusions associated with less or incomplete organic coatings. The inorganic inclusions (likely sulfate and sea salts) of B2 and B4 samples might have initiated ice nucleation at ~10% RH_{ice} higher than the laboratory-generated ammonium sulfate [*Abbatt et al.*, 2006; *Shilling et al.*, 2006; *Wise et al.*, 2010], NaCl [*Wise et al.*, 2012], and hydrated NaCl [*Wise et al.*, 2012] particles. The differences in RH_{ice} onsets could be due to the small size or surface area of uncoated inclusions compared to the laboratory-generated ammonium sulfate and NaCl particles [*Kanji et al.*, 2008]. The inorganic inclusions of B2 and B4 samples may exist in a crystalline state and/or penetrate the organic coating and thus may provide more active sites than A2, A3, and A4 samples which possess thicker organic coatings with a smoother surface structure. In turn, this renders more efficient deposition ice nucleation in the marine influenced B2 and B4 samples containing less organics, as compared to A2, A3, and A4 samples which were dominated by anthropogenic organic particles. The crystalline state and corresponding surface irregularities of metal-containing M1 sample may also provide additional ice nucleation sites.

[43] The observed differences in deposition ice nucleation efficiencies of A and B samples indicate that the physical and morphology of coating and inclusions may be important factors controlling deposition ice nucleation of both anthropogenic and marine influenced particles. However, these factors may ultimately depend on the chemical nature of the particle compounds which governs the phase state at these low temperatures.

4. Conclusions

[44] CCSEM/EDX and STXM/NEXAFS micro-spectroscopy methods of chemical imaging analyses provided physical and chemical characterization of individual particles collected during the CalNex and MILAGRO field studies, including particle size, morphology, coating, composition, and mixing state. Particles collected on May 19 (A samples) in Los Angeles mainly consisted of soot and secondary organic material, whereas on May 23 (B samples) the majority of particles consisted of inorganic cores thinly coated with organic material. M1 sample collected in Mexico City was dominated by Pb/Zn-containing particles apportioned to waste incineration emissions. The chemical composition and meteorological data suggested that A and B samples most likely were influenced by anthropogenic and marine sources, respectively.

[45] Particles from anthropogenic organic dominated (A2 and A3) and marine inorganic dominated (B2 and B4) samples took up water and exhibited high immersion freezing efficiencies above 230 K. The ambient particles with soot or other insoluble inclusions can nucleate ice and affect lower troposphere cloud formation, e.g., mixed-phase cloud formation. For example, A3 and B2 particle samples can nucleate ice at subsaturated conditions and deplete the liquid water content due to Bergeron-Wegener-Findeisen process. The presented data also demonstrate that particles emitted from waste incineration may serve as efficient IN via immersion freezing. Therefore, these particles could also initiate ice formation under conditions of mixed-phase clouds [*Cziczo et al.*, 2009]. Thus, this particle type generated by human activities, such as coal combustion, smelting, and waste incineration, might have impacts on ice cloud formation on a regional scale and mesoscale, thereby affecting climate.

[46] The chemical composition of anthropogenic and marine influenced particles affects the onsets of water uptake and immersion freezing in the temperature range of 230–255 K relevant to mixed-phase cloud formation. Aged particles with greater extent of carboxylic functional groups are likely more hydrophilic and thus take up water at lower *RH*. The insoluble inclusions of the particles most likely cause the differences in immersion freezing efficiencies for the investigated samples. For deposition ice nucleation at temperatures relevant to cirrus cloud formation, particle physical properties and morphologies may play an important role in controlling the ice nucleation efficiency. Thus, the particles' chemical and physical properties have different effects on corresponding ice nucleation mode at different temperature regimes.

[47] Our observations suggest that ice nucleation may be not necessarily initiated by particles with highest ice nucleation propensities present at very low number concentrations, as commonly assumed. Instead, particles with mediocre ice nucleation propensity but present at high number concentrations in the atmosphere can play an equivalently important role. In a typical atmospheric environment with a variety of complex mixture of airborne particles, the likelihood that efficient IN, such as mineral dust particles, are present in sufficient numbers and corresponding total particle surface areas is low and thus may play a smaller role in nucleation of atmospheric ice, except for special instances such as dust storm events. For these reasons, to comprehensively understand all atmospheric ice nucleation pathways, not only the most efficient IN has to be identified but also IN with lower nucleation efficiencies but present in higher number concentrations must be considered since those may surpass the most efficient IN in the glaciation process.

[48] The presented ice nucleation data demonstrate that anthropogenic affected and marine influenced particles with various chemical and physical properties exhibit distinctly different ice nucleation efficiencies and can serve as efficient IN at atmospheric conditions typical for cirrus and mixed phase clouds. The presented data indicate the potential link between human activities, particle composition, and ice cloud formation processes, and thus climate. The observed ice nucleation of anthropogenic and marine influenced particles provides further support to our previous finding that laboratory-generated surrogates do not exhibit ice nucleation properties representative of real ambient particles [*Knopf et al.*, 2010]. Clearly, more ice nucleation studies using field-collected particles combined with in-depth analyses of particle chemical and physical properties are necessary to assess their impact on atmospheric ice crystal formation and subsequent effects on the hydrological cycle and climate. The development of novel analytical techniques capable of observation of ice nucleation at the nano scale is needed to detect individual ice nucleation sites and to investigate the effects of chemical composition and morphological features of particles.

[49] **Acknowledgments.** B. Wang and D. A. Knopf acknowledge major support by the NOAA Climate Program Office, Atmospheric Composition and Climate Program, grant NA08OAR4310545, and partial support by the Atmospheric Chemistry Program of the National Science

Foundation (NSF) grant AGS-0846255. A. Laskin acknowledges support by Laboratory Directed Research and Development funds of Pacific Northwest National Laboratory (PNNL). Primary support for M. K. Gilles and the ALS-MES Beamline was provided by the Director, Office of Science, Office of Basic Energy Sciences, Division of Chemical Sciences, Geosciences, and Biosciences of the U. S. Department of Energy at Lawrence Berkeley National Laboratory under contract DE-AC02-05CH11231. A. Tivanski gratefully acknowledges support from the NOAA Climate Program Office, Earth System Science Program, award NA11OAR4310187. T. Roedel thanks the student exchange program between the University of Würzburg and U. C. Berkeley (curator A. Forchel, Würzburg and NSF IGERT program at UCB, DGE-0333455, Nanoscale Science and Engineering-From Building Blocks to Functional Systems). The Advanced Light Source is supported by the Director, Office of Science, Office of Basic Energy Sciences, of the U.S. Department of Energy under contract DE-AC02-05CH11231. The CCSEM/EDX particle analysis was performed at the William R. Wiley Environmental Molecular Sciences Laboratory, a national scientific user facility sponsored by the DOE's Office of Biological and Environmental Research and located at PNNL. PNNL is operated for the U.S. Department of Energy by Battelle Memorial Institute under contract DE-AC06-76RLO1830. We acknowledge sample collection by N. Levac, T. Nguyen, A. Bateman, D. Bones, and S. Nizkorodov during CalNex campaign and Y. Desyaterik and R. Hopkins during MILAGRO campaign. We thank P. Alpert for helpful discussions on this manuscript. We thank S. Newman for providing the meteorological data and P. L. Hayes and J. L. Jimenez for providing SMPS data for the dates of May 19 and 23.

References

Abbatt, J. P. D., S. Benz, D. J. Cziczo, Z. Kanji, U. Lohmann, and O. Möhler (2006), Solid ammonium sulfate aerosols as ice nuclei: A pathway for cirrus cloud formation, *Science*, *313*, 1770–1773.

Adachi, K., E. J. Freney, and P. R. Buseck (2011), Shapes of internally mixed hygroscopic aerosol particles after deliquescence, and their effect on light scattering, *Geophys. Res. Lett.*, *38*, L13804, doi:10.1029/2011GL047540.

Akhter, M. S., A. R. Chughtai, and D. M. Smith (1985), The structure of hexane soot I: Spectroscopic studies, *Appl. Spectrosc.*, *39*(1), 143–153, doi:10.1366/0003702854249114.

Albrecht, B. (1989), Aerosols, cloud microphysics and fractional cloudiness, *Science*, *245*, 1227–1230, doi:10.1126/science.245.4923.1227.

Avramov, A., and J. Y. Harrington (2010), Influence of parameterized ice habit on simulated mixed phase Arctic clouds, *J. Geophys. Res.*, *115*, D03205, doi:10.1029/2009JD012108.

Bailey, M., and J. Hallett (2004), Growth rates and habits of ice crystals between −20°C and −70°C, *J. Atmos. Sci.*, *61*(5), 514–544, doi:10.1175/1520-0469(2004)061<0514:GRAHOI>2.0.CO;2.

Baker, M. B. (1997), Cloud microphysics and climate, *Science*, *276*, 1072–1078, doi:10.1126/science.276.5315.1072.

Baker, M. B., and T. Peter (2008), Small-scale cloud processes and climate, *Nature*, *451*, 299–300, doi:10.1038/nature06594.

Baustian, K. J., D. J. Cziczo, M. E. Wise, K. A. Pratt, G. Kulkarni, A. G. Hallar, and M. A. Tolbert (2012), Importance of aerosol composition, mixing state, and morphology for heterogeneous ice nucleation: A combined field and laboratory approach, *J. Geophys. Res.*, *117*, D06217, doi:10.1029/2011JD016784.

Borys, R. D., and R. A. Duce (1979), Relationships among lead, iodine, trace metals and ice nuclei in a coastal urban atmosphere, *J. Appl. Meteorol.*, *18*(11), 1490–1494.

Braban, C. F., J. P. D. Abbatt, and D. J. Cziczo (2001), Deliquescence of ammonium sulfate particles at sub-eutectic temperatures, *Geophys. Res. Lett.*, *28*(20), 3879–3882.

Cantrell, W., and A. Heymsfield (2005), Production of ice in tropospheric clouds, *Bull. Am. Meteorol. Soc.*, *86*(6), 795–807, doi:10.1175/BAMS-86-6-795.

Chen, T., W. B. Rossow, and Y. Zhang (2000), Radiative effects of cloud-type variations, *J. Clim.*, *13*(1), 264–286, doi:10.1175/1520-0442(2000)013<0264:REOCTV>2.0.CO;2.

Chen, Y., S. M. Kreidenweis, L. M. McInnes, D. C. Rogers, and P. J. DeMott (1998), Single particle analyses of ice nucleating aerosols in the upper troposphere and lower stratosphere, *Geophys. Res. Lett.*, *25*(9), 1391–1394, doi:10.1029/97GL03261.

Chou, C., O. Stetzer, T. Tritscher, R. Chirico, M. F. Heringa, Z. A. Kanji, E. Weingartner, A. S. H. Prévôt, U. Baltensperger, and U. Lohmann (2012), Effect of photochemical aging on the ice nucleation properties of diesel and wood burning particles, *Atmos. Chem. Phys. Discuss.*, *12*(6), 14,697–14,726, doi:10.5194/acpd-12-14697-2012.

Chughtai, A. R., J. A. Jassim, J. H. Peterson, D. H. Stedman, and D. M. Smith (1991), Spectroscopic and solubility characteristics of oxidized soots, *Aerosol Sci. Technol.*, *15*(2), 112–126, doi:10.1080/02786829108959518.

Cozic, J., S. Mertes, B. Verheggen, D. J. Cziczo, S. J. Gallavardin, U. S. Walter, Baltensperger, and E. Weingartner (2008), Black carbon enrichment in atmospheric ice particle residuals observed in lower tropospheric mixed phase clouds, *J. Geophys. Res.*, *113*, D15209, doi:10.1029/2007JD009266.

Cziczo, D. J., and J. P. D. Abbatt (2000), Infrared observations of the response of NaCl, $MgCl_2$, NH_4HSO_4, and NH_4NO_3 aerosols to changes in relative humidity from 298 to 238 K, *J. Phys. Chem. A*, *104*, 2038–2047.

Cziczo, D. J., D. M. Murphy, P. K. Hudson, and D. S. Thomson (2004), Single particle measurements of the chemical composition of cirrus ice residue during CRYSTAL-FACE, *J. Geophys. Res.*, *109*, D04201, doi:10.1029/2003JD004032.

Cziczo, D. J., et al. (2009), Inadvertent climate modification due to anthropogenic lead, *Nat. Geosci.*, *2*(5), 333–336.

Daly, H. M., and A. B. Horn (2009), Heterogeneous chemistry of toluene, kerosene and diesel soots, *Phys. Chem. Chem. Phys.*, *11*, 1069–1076, doi:10.1039/B815400G.

DeMott, P. J. (1990), An exploratory study of ice nucleation by soot aerosols, *J. Appl. Meteorol.*, *29*, 1072–1079.

DeMott, P. J., D. J. Cziczo, A. J. Prenni, D. M. Murphy, S. M. Kreidenweis, D. S. Thomson, R. Borys, and D. C. Rogers (2003), Measurements of the concentration and composition of nuclei for cirrus formation, *Proc. Natl. Acad. Sci. U. S. A.*, *100*(25), 14,655–14,660, doi:10.1073/pnas.2532677100.

DeMott, P. J., A. J. Prenni, X. Liu, S. M. Kreidenweis, M. D. Petters, C. H. Twohy, M. S. Richardson, T. Eidhammer, and D. C. Rogers (2010), Predicting global atmospheric ice nuclei distributions and their impacts on climate, *Proc. Natl. Acad. Sci. U. S. A.*, *107*(25), 11,217–11,222, doi:10.1073/pnas.0910818107.

Detwiler, A. G., and V. Bernard (1981), Humidity required for ice nucleation from the vapor onto silver iodide and lead iodide aerosols over the temperature range −6 to −67°C, *J. Appl. Meteorol.*, *20*, 1006–1012.

Diehl, K., and S. K. Mitra (1998), A laboratory study of the effects of a kerosene-burner exhaust on ice nucleation and the evaporation rate of ice crystals, *Atmos. Environ.*, *32*, 3145–3151.

Dymarska, M., B. J. Murray, L. M. Sun, M. L. Eastwood, D. A. Knopf, and A. K. Bertram (2006), Deposition ice nucleation on soot at temperatures relevant for the lower troposphere, *J. Geophys. Res.*, *111*, D04204, doi:10.1029/2005JD006627.

Eastwood, M. L., S. Cremel, C. Gehrke, E. Girard, and A. K. Bertram (2008), Ice nucleation on mineral dust particles: Onset conditions, nucleation rates and contact angles, *J. Geophys. Res.*, *113*, D22203, doi:10.1029/2008JD010639.

Ebert, M., A. Worringen, N. Benker, S. Mertes, E. Weingartner, and S. Weinbruch (2011), Chemical composition and mixing-state of ice residuals sampled within mixed phase clouds, *Atmos. Chem. Phys.*, *11*(6), 2805–2816, doi:10.5194/acp-11-2805-2011.

Fornea, A. P., S. D. Brooks, J. B. Dooley, and A. Saha (2009), Heterogeneous freezing of ice on atmospheric aerosols containing ash, soot, and soil, *J. Geophys. Res.*, *114*, D13201, doi:10.1029/2009JD011958.

Forster, P., et al. (2007), Changes in atmospheric constituents and in radiative forcing, in *Climate Change 2007: The Physical Science Basis. Contribution of Working Group I to the Fourth Assessment Report of the Intergovernmental Panel on Climate Change*, pp. 131–234, Cambridge Univ. Press, New York.

Friedman, B., G. Kulkarni, J. B. Welti, A. Zelenyuk, J. A. Thornton, and D. J. Cziczo (2011), Ice nucleation and droplet formation by bare and coated soot particles, *J. Geophys. Res.*, *116*, D17203, doi:10.1029/2011JD015999.

Froyd, K. D., D. M. Murphy, P. Lawson, D. Baumgardner, and R. L. Herman (2010), Aerosols that form subvisible cirrus at the tropical tropopause, *Atmos. Chem. Phys.*, *10*(1), 209–218, doi:10.5194/acp-10-209-2010.

Fuzzi, S., et al. (2006), Critical assessment of the current state of scientific knowledge, terminology, and research needs concerning the role of organic aerosols in the atmosphere, climate, and global change, *Atmos. Chem. Phys.*, *6*(7), 2017–2038, doi:10.5194/acp-6-2017-2006.

Garten, V. A., and R. B. Head (1964), Carbon particles and ice nucleation, *Nature*, *201*, 1091–1092, doi:10.1038/2011091a0.

George, I. J., and J. P. D. Abbatt (2010), Heterogeneous oxidation of atmospheric aerosol particles by gas-phase radicals, *Nat. Chem.*, *2*(9), 713–722, doi:10.1038/nchem.806.

Ghorai, S., and A. V. Tivanski (2010), Hygroscopic behavior of individual submicrometer particles studied by X-ray spectromicroscopy, *Anal. Chem.*, *82*(22), 9289–9298, doi:10.1021/ac101797k.

Ghorai, S., A. Laskin, and A. V. Tivanski (2011), Spectroscopic evidence of keto-enol tautomerism in deliquesced malonic acid particles, *J. Phys. Chem. A*, *115*(17), 4373–4380, doi:10.1021/jp112360x.

Gorbunov, B., and A. Safatov (1994), In-situ measurements of the ice-forming activity of metal-oxide aerosols with controlled amounts of surface-active groups, *J. Aerosol. Sci.*, *25*(4), 673–682.

Gorbunov, B., A. Baklanov, N. Kakutkina, H. L. Windsor, and R. Toumi (2001), Ice nucleation on soot particles, *J. Aerosol. Sci.*, *32*(2), 199–215.

Hallett, J., W. P. Arnott, M. P. Bailey, and J. T. Hallett (2002), Ice crystals in cirrus, in *Cirrus*, edited by K. D. Lynch et al., chap. 3, pp. 41–77, Oxford Univ. Press, New York.

Hallquist, M., et al. (2009), The formation, properties and impact of secondary organic aerosol: Current and emerging issues, *Atmos. Chem. Phys.*, *9*(14), 5155–5236, doi:10.5194/acp-9-5155-2009.

Held, I. M., and B. J. Soden (2000), Water vapor feedback and global warming, *Annu. Rev. Energy Environ.*, *25*, 441–475.

Jang, M. S., N. M. Czoschke, S. Lee, and R. M. Kamens (2002), Heterogeneous atmospheric aerosol production by acid-catalyzed particle-phase reactions, *Science*, *298*(5594), 814–817, doi:10.1126/science.1075798.

Jensen, E. J., and O. B. Toon (1997), The potential impact of soot particles from aircraft exhaust on cirrus clouds, *Geophys. Res. Lett.*, *24*(3), 249–252.

Jimenez, J. L., et al. (2009), Evolution of organic aerosols in the atmosphere, *Science*, *326*(5959), 1525–1529, doi:10.1126/science.1180353.

Johnson, K. S., B. Zuberi, L. T. Molina, M. J. Molina, M. J. Iedema, J. P. Cowin, D. J. Gaspar, C. Wang, and A. Laskin (2005), Processing of soot in an urban environment: Case study from the Mexico City metropolitan area, *Atmos. Chem. Phys.*, *5*(D4), 3033–3043.

Jost, H. J., et al. (2004), In-situ observations of mid-latitude forest fire plumes deep in the stratosphere, *Geophys. Res. Lett.*, *31*, L11101, doi:10.1029/2003GL019253.

Kaiser, J. C., N. Riemer, and D. A. Knopf (2011), Detailed heterogeneous oxidation of soot surfaces in a particle-resolved aerosol model, *Atmos. Chem. Phys.*, *11*(9), 4505–4520, doi:10.5194/acp-11-4505-2011.

Kanakidou, M., et al. (2005), Organic aerosol and global climate modelling: A review, *Atmos. Chem. Phys.*, *5*(4), 1053–1123, doi:10.5194/acp-5-1053-2005.

Kanji, Z. A., and J. P. D. Abbatt (2006), Laboratory studies of ice formation via deposition mode nucleation onto mineral dust and n-hexane soot samples, *J. Geophys. Res.*, *111*, D16204, doi:10.1029/2005JD006766.

Kanji, Z. A., and J. P. D. Abbatt (2010), Ice nucleation onto Arizona Test Dust at cirrus temperatures: Effect of temperature and aerosol size on onset relative humidity, *J. Phys. Chem. A*, *114*(2), 935–941, doi:10.1021/jp908661m.

Kanji, Z. A., O. Florea, and J. P. D. Abbatt (2008), Ice formation via deposition nucleation on mineral dust and organics: Dependence of onset relative humidity on total particulate surface area, *Environ. Res. Lett.*, *3*(2), 025004, doi:10.1088/1748-9326/3/2/025004.

Kärcher, B., and J. Ström (2003), The roles of dynamical variability and aerosols in cirrus cloud formation, *Atmos. Chem. Phys.*, *3*(3), 823–838, doi:10.5194/acp-3-823-2003.

Kilcoyne, A. L. D., et al. (2003), Interferometer-controlled scanning transmission X-ray microscopes at the Advanced Light Source, *J. Synchrotron Radiat.*, *10*(2), 125–136, doi:10.1107/S0909049502017739.

Knopf, D. A., and S. M. Forrester (2011), Heterogeneous ice nucleation from water and aqueous NaCl droplets coated by 1-nonadecanol and 1-nonadecanoic acid monolayers, *J. Phys. Chem. A*, *115*, 5579–5591.

Knopf, D. A., and T. Koop (2006), Heterogeneous nucleation of ice on surrogates of mineral dust, *J. Geophys. Res.*, *111*, D12201, doi:10.1029/2005JD006894.

Knopf, D. A., and M. D. Lopez (2009), Homogeneous ice freezing temperatures and ice nucleation rates of aqueous ammonium sulfate and aqueous levoglucosan particles for relevant atmospheric conditions, *Phys. Chem Chem. Phys.*, *11*, 8056–8068, doi:10.1039/b903750k.

Knopf, D. A., J. Mak, S. Gross, and A. K. Bertram (2006), Does atmospheric processing of saturated hydrocarbon surfaces by NO_3 lead to volatilization?, *Geophys. Res. Lett.*, *33*, L17816, doi:10.1029/2006GL026884.

Knopf, D. A., B. Wang, A. Laskin, R. C. Moffet, and M. K. Gilles (2010), Heterogeneous nucleation of ice on anthropogenic organic particles collected in Mexico City, *Geophys. Res. Lett.*, *37*, L11803, doi:10.1029/2010GL043362.

Knopf, D. A., S. M. Forrester, and J. H. Slade (2011a), Heterogeneous oxidation kinetics of organic biomass burning aerosol surrogates by O_3, NO_2, N_2O_5, and NO_3, *Phys. Chem. Chem. Phys.*, *13*, 21,050–21,062, doi:10.1039/C1CP22478F.

Knopf, D. A., P. A. Alpert, B. Wang, and J. Y. Aller (2011b), Stimulation of ice nucleation by marine diatoms, *Nat. Geosci.*, *4*, 88–90, doi:10.1038/NGEO1037.

Koehler, K. A., P. J. DeMott, S. M. Kreidenweis, O. B. Popovicheva, M. D. Petters, C. M. Carrico, E. D. Kireeva, T. D. Khokhlovac, and N. K. Shonijac (2009), Cloud condensation nuclei and ice nucleation activity of hydrophobic and hydrophilic soot particles, *Phys. Chem. Chem. Phys.*, *11*, 7906–7920, doi:10.1039/b905334b.

Koop, T., B. P. Luo, A. Tsias, and T. Peter (2000a), Water activity as the determinant for homogeneous ice nucleation in aqueous solutions, *Nature*, *406*, 611–614, doi:10.1038/35020537.

Koop, T., A. Kapilashrami, L. T. Molina, and M. J. Molina (2000b), Phase transitions of sea-salt/water mixtures at low temperatures: Implications for ozone chemistry in the polar marine boundary layer, *J. Geophys. Res.*, *105*(D21), 26,393–26,402.

Koop, T., J. Bookhold, M. Shiraiwa, and U. Pöschl (2011), Glass transition and phase state of organic compounds: Dependency on molecular properties and implications for secondary organic aerosols in the atmosphere, *Phys. Chem. Chem. Phys.*, *13*, 19,238–19,255, doi:10.1039/C1CP22617G.

Laskin, A., M. Iedema, and J. Cowin (2003), Time-resolved aerosol collector for CCSEM/EDX single-particle analysis, *Aerosol Sci. Technol.*, *37*(3), 246–260, doi:10.1080/02786820300945.

Laskin, A., J. P. Cowin, and M. J. Iedema (2006), Analysis of individual environmental particles using modern methods of electron microscopy and X-ray microanalysis, *J. Electron Spectrosc. Relat. Phenom.*, *150*(2–3), 260–274.

Lee, P. M. (2004), *Bayesian Statistics: An Introduction*, 3rd ed., John Wiley, Hoboken, N. J.

Levy, P. S., and S. Lemeshow (1991), Simple random sampling, in *Sampling of Populations: Methods and Application*, pp. 49–63, John Wiley, Hoboken, N. J.

Lohmann, U., and E. Roeckner (1995), Influence of cirrus cloud radiative forcing on climate and climate sensitivity in a general-circulation model, *J. Geophys. Res.*, *100*(D8), 16,305–16,323.

Massoli, P., et al. (2010), Relationship between aerosol oxidation level and hygroscopic properties of laboratory generated secondary organic aerosol (SOA) particles, *Geophys. Res. Lett.*, *37*, L24801, doi:10.1029/2010GL045258.

McFarquhar, G. M., G. Zhang, M. R. Poellot, G. L. Kok, R. McCoy, T. Tooman, A. Fridlind, and A. J. Heymsfield (2007), Ice properties of single-layer stratocumulus during the Mixed-Phase Arctic Cloud Experiment: 1. Observations, *J. Geophys. Res.*, *112*, D24201, doi:10.1029/2007JD008633.

Mikhailov, E., S. Vlasenko, S. T. Martin, T. Koop, and U. Pöschl (2009), Amorphous and crystalline aerosol particles interacting with water vapor: Conceptual framework and experimental evidence for restructuring, phase transitions and kinetic limitations, *Atmos. Chem. Phys.*, *9*(24), 9491–9522.

Moffet, R. C., et al. (2008), Characterization of aerosols containing Zn, Pb, and Cl from an industrial region of Mexico City, *Environ. Sci. Technol.*, *42*(19), 7091–7097.

Moffet, R. C., et al. (2010a), Microscopic characterization of carbonaceous aerosol particle aging in the outflow from Mexico City, *Atmos. Chem. Phys.*, *10*(3), 961–976.

Moffet, R. C., T. Henn, A. Laskin, and M. K. Gilles (2010b), Automated chemical analysis of internally mixed aerosol particles using X-ray spectromicroscopy at the carbon k-edge, *Anal. Chem.*, *82*(19), 7906–7914, doi:10.1021/ac1012909.

Moffet, R. C., A. V. Tivanski, and M. K. Gilles (2010c), Scanning transmission X-ray microscopy: Applications in atmospheric aerosol research, in *Fundamentals and Applications in Aerosol Spectroscopy*, edited by R. Signorell and J. P. Reid, pp. 419–462, Taylor and Francis, Philadelphia, Pa.

Möhler, O., et al. (2005), Effect of sulfuric acid coating on heterogeneous ice nucleation by soot aerosol particles, *J. Geophys. Res.*, *110*, D11210, doi:10.1029/2004JD005169.

Möhler, O., S. Benz, H. Saathoff, M. Schnaiter, R. Wagner, J. Schneider, S. Walter, V. Ebert, and S. Wagner (2008), The effect of organic coating on the heterogeneous ice nucleation efficiency of mineral dust aerosols, *Environ. Res. Lett.*, *3*(2), 1425–1435.

Molina, L. T., S. Madronich, J. S. Gaffney, H. B. Singh, and U. Pöschl (Eds.) (2007), ACP special issue: MILAGRO/INTEX-B 2006, *Atmos. Chem. Phys.*, *7*, 2160 pp.

Murphy, D. M., and T. Koop (2005), Review of the vapour pressures of ice and supercooled water for atmospheric applications, *Q. J. R. Meteorol. Soc.*, *131*(608), 1539–1565, doi:10.1256/qj.04.94.

Murphy, D. M., D. S. Thomson, and T. M. J. Mahoney (1998), In situ measurements of organics, meteoritic material, mercury, and other elements in aerosols at 5 to 19 kilometers, *Science*, *282*, 1664–1669, doi:10.1126/science.282.5394.1664.

Murphy, D. M., D. J. Cziczo, P. K. Hudson, and D. S. Thomson (2007a), Carbonaceous material in aerosol particles in the lower stratosphere and tropopause region, *J. Geophys. Res.*, *112*, D04203, doi:10.1029/2006JD007297.

Murphy, D. M., et al. (2007b), Distribution of lead in single atmospheric particles, *Atmos. Chem. Phys.*, *7*(12), 3195–3210, doi:10.5194/acp-7-3195-2007.

Murray, B. J. (2008), Inhibition of ice crystallisation in highly viscous aqueous organic acid droplets, *Atmos. Chem. Phys.*, *8*(17), 5423–5433, doi:10.5194/acp-8-5423-2008.

Murray, B. J., et al. (2010), Heterogeneous nucleation of ice particles on glassy aerosols under cirrus conditions, *Nat. Geosci.*, *3*, 233–237.

Niedermeier, D., et al. (2011), Experimental study of the role of physicochemical surface processing on the IN ability of mineral dust particles, *Atmos. Chem. Phys.*, *11*(21), 11,131–11,144, doi:10.5194/acp-11-11131-2011.

Onasch, T. B., R. L. Siefert, S. D. Brooks, A. J. Prenni, B. Murray, M. A. Wilson, and M. A. Tolbert (1999), Infrared spectroscopic study of the deliquescence and efflorescence of ammonium sulfate aerosol as a function of temperature, *J. Geophys. Res.*, *104*(D17), 21,317–21,326.

Parsons, M. T., D. A. Knopf, and A. K. Bertram (2004), Deliquescence and crystallization of ammonium sulfate particles internally mixed with water-soluble organic compounds, *J. Phys. Chem. A*, *108*(52), 11,600–11,608.

Popovicheva, O., E. Kireeva, N. Persiantseva, T. Khokhlova, N. Shonija, V. Tishkova, and B. Demirdjian (2008), Effect of soot on immersion freezing of water and possible atmospheric implications, *Atmos. Res.*, *90*(2–4), 326–337, doi:10.1016/j.atmosres.2008.08.004.

Prenni, A. J., P. J. Demott, D. C. Rogers, S. M. Kreidenweis, G. M. McFarquhar, G. Zhang, and M. R. Poellot (2009a), Ice nuclei characteristics from M-PACE and their relation to ice formation in clouds, *Tellus, Ser. B*, *61*(2), 436–448, doi:10.1111/j.1600-0889.2009.00415.x.

Prenni, A. J., M. D. Petters, A. Faulhaber, C. M. Carrico, P. J. Ziemann, S. M. Kreidenweis, and P. J. DeMott (2009b), Heterogeneous ice nucleation measurements of secondary organic aerosol generated from ozonolysis of alkenes, *Geophys. Res. Lett.*, *36*, L06808, doi:10.1029/2008GL036957.

Pruppacher, R. H., and J. D. Klett (1997), *Microphysics of Clouds and Precipitation*, Kluwer Acad., Dordrecht, Netherlands.

Ramanathan, V., P. J. Crutzen, J. T. Kiehl, and D. Rosenfeld (2001), Aerosols, climate, and the hydrological cycle, *Science*, *294*(5549), 2119–2124, doi:10.1126/science.1064034.

Riemer, N., H. Vogel, and B. Vogel (2004), Soot aging time scales in polluted regions during day and night, *Atmos. Chem. Phys.*, *4*, 1885–1893.

Rosenfeld, D. (2000), Suppression of rain and snow by urban and industrial air pollution, *Science*, *287*(5459), 1793–1796, doi:10.1126/science.287.5459.1793.

Rudich, Y., N. M. Donahue, and T. F. Mentel (2007), Aging of organic aerosol: Bridging the gap between laboratory and field studies, *Annu. Rev. Phys. Chem.*, *58*, 321–352, doi:10.1146/annurev.physchem.58.032806.104432.

Schill, G. P., and M. A. Tolbert (2012), Depositional ice nucleation on monocarboxylic acids: Effect of the O:C ratio, *J. Phys. Chem. A*, *116*(25), 6817–6822, doi:10.1021/jp301772q.

Seinfeld, J. H., and S. N. Pandis (1998), *Atmospheric Chemistry and Physics*, John Wiley, Hoboken, N. J.

Shilling, J. E., T. J. Fortin, and M. A. Tolbert (2006), Depositional ice nucleation on crystalline organic and inorganic solids, *J. Geophys. Res.*, *111*, D12204, doi:10.1029/2005JD006664.

Smith, D., W. Welch, J. Jassim, A. Chughtai, and D. Stedman (1988), Soot-ozone reaction kinetics: spectroscopic and gravimetric studies, *Appl. Spectrosc.*, *42*(8), 1473–1482, doi:10.1366/0003702884429779.

Springmann, M., D. A. Knopf, and N. Riemer (2009), Detailed heterogeneous chemistry in an urban plume box model: Reversible co-adsorption of O_3, NO_2, and H_2O on soot coated with benzo[a]pyrene, *Atmos. Chem. Phys.*, *9*(19), 7461–7479, doi:10.5194/acp-9-7461-2009.

Sullivan, R. C., L. Minambres, P. J. DeMott, A. J. Prenni, C. M. Carrico, E. J. T. Levin, and S. M. Kreidenweis (2010), Chemical processing does not always impair heterogeneous ice nucleation of mineral dust particles, *Geophys. Res. Lett.*, *37*, L24805, doi:10.1029/2010GL045540.

Thompson, S. (1987), Sample-size for estimating multinomial proportions, *Am. Stat.*, *41*(1), 42–46, doi:10.2307/2684318.

Twomey, S. (1974), Pollution and planetary albedo, *Atmos. Environ.*, *8*(12), 1251–1256, doi:10.1016/j.atmosenv.2007.10.062.

Vali, G. (1985), Nucleation terminology, *J. Aerosol Sci.*, *16*(6), 575–576, doi:10.1016/0021-8502(85)90009-6.

Veres, P. R., et al. (2011), Evidence of rapid production of organic acids in an urban air mass, *Geophys. Res. Lett.*, *38*, L17807, doi:10.1029/2011GL048420.

Verlinde, J., et al. (2007), The mixed-phase arctic cloud experiment, *Bull. Am. Meteorol. Soc.*, *88*(2), 205–221, doi:10.1175/BAMS-88-2-205.

Virtanen, A., et al. (2010), An amorphous solid state of biogenic secondary organic aerosol particles, *Nature*, *467*(7317), 824–827, doi:10.1038/nature09455.

Wang, B., and D. A. Knopf (2011), Heterogeneous ice nucleation on particles composed of humic–like substances impacted by O_3, *J. Geophys. Res.*, *116*, D03205, doi:10.1029/2010JD014964.

Wang, B., A. T. Lambe, P. Massoli, T. B. Onasch, P. Davidovits, D. R. Worsnop, and D. A. Knopf (2012), The deposition ice nucleation and immersion freezing potential of amorphous secondary organic aerosol: Pathways for ice and mixed-phase cloud formation, *J. Geophys. Res.*, *117*, D16209, doi:10.1029/2012JD018063.

Welti, A., F. Lüönd, and U. Lohmann (2009), Influence of particle size on the ice nucleating ability of mineral dusts, *Atmos. Chem. Phys.*, *9*(18), 6705–6715, doi:10.5194/acp-9-6705-2009.

Wise, M. E., K. J. Baustian, and M. A. Tolbert (2010), Internally mixed sulfate and organic particles as potential ice nuclei in the tropical tropopause region, *Proc. Natl. Acad. Sci. U. S. A.*, *107*(15), 6693–6698, doi:10.1073/pnas.0913018107.

Wise, M. E., K. J. Baustian, T. Koop, M. A. Freedman, E. J. Jensen, and M. A. Tolbert (2012), Depositional ice nucleation onto crystalline hydrated NACL particles: A new mechanism for ice formation in the troposphere, *Atmos. Chem. Phys.*, *12*(2), 1121–1134, doi:10.5194/acp-12-1121-2012.

Zhang, Q., et al. (2007), Ubiquity and dominance of oxygenated species in organic aerosols in anthropogenically-influenced Northern Hemisphere midlatitudes, *Geophys. Res. Lett.*, *34*, L13801, doi:10.1029/2007GL029979.

Zobrist, B., C. Marcolli, T. Peter, and T. Koop (2008), Heterogeneous ice nucleation in aqueous solutions: the role of water activity, *J. Phys. Chem. A*, *112*(17), 3965–3975.

Zobrist, B., V. Soonsin, B. P. Luo, U. K. Krieger, C. Marcolli, T. Peter, and T. Koop (2011), Ultra-slow water diffusion in aqueous sucrose glasses, *Phys. Chem. Chem. Phys.*, *13*, 3514–3526, doi:10.1039/C0CP01273D.

Zuberi, B., K. S. Johnson, G. K. Aleks, L. T. Molina, and A. Laskin (2005), Hydrophilic properties of aged soot, *Geophys. Res. Lett.*, *32*, L01807, doi:10.1029/2004GL021496.